Bulletin of Earthquake Engineering
https://doi.org/10.1007/s10518-021-01054-8

ORIGINAL ARTICLE

An updated probabilistic seismic hazard assessment (PSHA) for Pakistan

Asad ur Rahman[1] · Fawad Ahmed Najam[1] · Saeed Zaman[2] · Atif Rasheed[1] · Irfan Ahmad Rana[1]

Received: 27 April 2020 / Accepted: 1 February 2021

Abstract

In this study, an updated probabilistic seismic hazard assessment (PSHA) of Pakistan region is performed using the procedures developed for the US National Seismic Hazard Maps and the Earthquake Model of the Middle East (EMME14). It is based on the combination of conventional area sources model and the spatially smoothed gridded seismicity model with crustal faults. An updated earthquake catalogue is compiled using several international and national databases. The background seismicity of the study area is modeled using both the area source zones and the spatially smoothed gridded seismicity approach. A total of 110 crustal fault sources are modeled using their geological slip rates obtained from the database developed by the Global Earthquake Model (GEM). The Makran Subduction Zone (MSZ) is also modeled using a combination of inclined area source zone and the spatially smoothed seismicity approach. Several Ground Motion Prediction Equations (GMPEs) developed by the PEER Next Generation Attenuation (NGA) initiative are employed to estimate the hazard at bedrock level. The logic tree procedure is used to deal with the epistemic uncertainties associated with the source models and the GMPEs. The updated hazard maps for the Peak Ground Acceleration (PGA) and Spectral Accelerations (SA) at natural periods of 0.2 s, 1 s and 2 s are developed for the 10% and 2% probability of exceedance in 50 years (DBE and MCE levels, respectively). The hazard curves and Uniform Hazard Spectra (UHS) for several major cities of Pakistan are also presented. The results provide an updated understanding of the seismic hazard in Pakistan. The presented hazard maps, curves and spectra can be used for the structural design of new buildings as well as the performance assessment of existing buildings. They also provide an improved basis for the policy formulation and planning for effective disaster risk reduction in the region.

Keywords Pakistan · Kashmir · Karachi · Makran subduction zone · Islamabad · Hazard maps · Uniform hazard spectra · Peak ground acceleration

✉ Asad ur Rahman
asadjan1801@gmail.com

[1] National University of Sciences and Technology (NUST), Islamabad, Pakistan

[2] University of Engineering and Technology (UET), Jalozai Campus, Peshawar, Pakistan

1 Introduction

Pakistan and surrounding areas are a seismically active and earthquake-prone region of the world. The northeastern part of the country lies on the active Himalayan orogenic belt which is created by a slow collision between Eurasian and Indian plates spanning from the past 30 to 40 million years (Aitchison et al. 2007). The seismicity of southwestern part of the country is also characterized by a complex network of active crustal faults spread around the main plate boundary. This complex seismo-tectonic environment of the region poses a high level of seismic hazard to the country and its neighboring areas. In the past, this region has been hit by several destructive earthquakes resulting in a huge number of fatalities (see Table 1). On the other hand, a rapid growth in population and unsustainable urbanization is also resulting in an increased seismic risk of the region.

As part of the attempts to mitigate the seismic risk, various efforts have been made in the past to calculate the likelihood of seismic ground shaking in the region. The first seismic hazard assessment for Pakistan was conducted in 1986 to develop a consistent seismic design criterion for inclusion in the Pakistan Building Code (PBC 1986). This study was based on a catalogue developed using instrumentally recorded earthquakes from 1905 to 1979 CE (Rossetto and Peiris 2009). Based on the hazard defined by the ranges of Modified Mercalli Intensity (MMI) scale, Pakistan was divided into four seismic zones (PBC 1986). Later, a more detailed probabilistic seismic hazard analysis (PSHA) was performed as part of the Global Seismic Hazard Assessment Program (GSHAP) (Giardini and Basham 1993; Giardini et al. 1999; Zhang et al. 1999). Under this program, the PSHA of Pakistan and surrounding region was carried out using the classical methodology established by Cornell (1968) and McGuire (1978). This methodology is based on the area source delineations and assumes a uniform seismicity rate in each seismic source zone. A basic limitation of this approach is that the results can be substantially influenced by the delineation of

Table 1 Some major earthquake events and the number of fatalities occurred in Pakistan and adjoining regions

Date	M_w	Location	Deaths	Source
24/09/2019	5.6	Mirpur, Azad Kashmir	38	(USGS 2019)
25/12/2015	6.3	Gilgith-Balthistan	4	
26/10/2015	7.5	Badakhshan, Afghanistan	399	
28/09/2013	6.8	Awaran, Balochistan	400	
24/09/2013	7.4	Awaran, Balochistan	825	
18/01/2011	7.2	Dalbandin, Balochistan	3	
29/10/2008	6.4	Ziarat, Balochistan	215	
08/09/2005	7.6	Balakot, Azad Kashmir	73,000	(Durrani 2005)
27/02/1997	7	Balochistan region	57	(ISC 2019)
28/12/1974	6.2	Khyber Pukhtunkhwa	5300	(Utsu 2002)
28/11/1945	8.2	Makran, Balochistan	300–600	
31/05/1935	7.7	Ali jaan, Balochistan	30,000–60,000	(Bangash 2011)
21/10/1909	7	Sibi, Balochistan	100	(Quittmeyer and Jacob 1979)
24/09/1827	7.8	Lahore, Punjab	1000	
16/06/1819	7.7–8.2	Allahbund, Sindh	> 1543	
02/05/1668	7.6	Sindh region	50,000	

seismic source zones, which are mainly based on the subjective judgment of the hazard analyst. In GSHAP (Giardini and Basham 1993; Giardini et al. 1999; Zhang et al. 1999), more than twenty seismic area sources were delineated for Pakistan and surrounded areas. The results were reported in the form of a hazard map presenting the peak ground acceleration (PGA) values corresponding to a return period of 475 years.

After the devastating M_w 7.6 Kashmir earthquake in 2005, the government of Pakistan took an initiative to develop the seismic provisions for updating the Pakistan Building Code (PBC 1986). The Ministry of Housing & Works (MOHW) assigned this task to National Engineering Services Pakistan (NESPAK), a leading consulting organization in the country. An updated PSHA (Shabbir and Ilyas 2007) of the country was performed using the methodology proposed by Cornell (1968) and McGuire (1978). The updated PGA map was developed as a result of this study. Following the code framework from the Uniform Building Code (UBC 1997), the country was divided into 5 zones (zone 1, 2A, 2B, 3 and 4) based on the PGA values. In 2007, this zonation map along with several seismic provisions, were included in an updated version of the Building Code of Pakistan (BCP 2007). Meanwhile, another detailed PSHA was performed by the *"Pakistan Meteorological Department (PMD)"* in cooperation with a research foundation *"Norwegian Seismic Array (NORSAR)"* (PMD and NORSAR 2007). Based on the conventional methodology (Cornell 1968; McGuire 1978), 19 seismic area sources were delineated in this study. Moreover, the seismicity of Hindukush region was also classified into shallow, intermediate and deep layers (0–30 km, 30–120 km and 120–300 km). The values of PGA and spectral acceleration (SA) at the natural periods of 0.2, 0.5, 1.0 and 2.0 s were reported for the return periods of 50, 100, 200, 500 and 1000 years.

In last decade, several improved PSHA studies were conducted to assess the seismic hazard of Pakistan and surrounding areas. Ali (2011) used the conventional Cornel-McGuire methodology (Cornell 1968; McGuire 1978) to develop the updated seismic hazard maps of Pakistan. Later, Zaman et al. (2012) also conducted a detailed PSHA study to develop a comprehensive set of hazard maps, hazard curves and uniform hazard spectra for various regions of Pakistan. In this study, the procedure used to develop the US national seismic hazard maps (NSHMP) (Petersen et al. 2008) was adopted. This procedure includes the spatially smoothed gridded seismicity approach (Frankel 1995) which has been successfully applied in other countries (Lapajne et al. 2003, 1997; Ornthammarath et al. 2011). Using an earthquake catalogue, this approach represents the hazard with spatially smoothed seismicity parameters in areas where the ruptured surface of crustal faults is not visible, or the potential seismic sources are mostly unidentified. However, the historical seismicity alone may not adequately represent the seismic hazard at lower probabilities of exceedance (e.g., for 2% probability of exceedance in 50 years). Therefore, in this study, some crustal faults having enough geological and paleoseismic evidence and slip rates were also modeled beside the smoothed seismicity. Moreover, the subduction source model for the Makran subduction zone (MSZ) was also included. More recently, the PSHA of Pakistan and surrounding region is also conducted as part of the Earthquake Model of Middle East (EMME) (Şeşetyan et al. 2018). In this study, a combination of spatially smoothed seismicity approach (Frankel 1995) and the conventional area sources approach were used to develop the hazard maps of the country.

In the current study, an updated probabilistic seismic hazard assessment (PSHA) of Pakistan is conducted using the spatially smoothed gridded seismicity approach and the conventional area sources approach (Danciu et al. 2018; Petersen et al. 2008, 2015). Several improvements have been made at each step of the PSHA methodology to develop a relatively reliable set of hazard maps, uniform hazard spectra and hazard curves for the

region. An updated earthquake catalogue is developed to model the spatially smoothed gridded seismicity and for the delineation of area sources. The Global Earthquake Model (GEM 2019) database of active faults is adopted to get the slip rates for modeling the crustal faults. The logic tree procedure is used to deal with the epistemic uncertainty in the hazard modelling. The PSHA is performed using two seismic source models (i.e. the conventional area sources, and the spatially smoothed seismicity with crustal faults). Equal weights of 0.5 are assigned to each model in the logic tree framework. The Makran subduction zone (MSZ) in the south is incorporated as an inclined rupture plane. The updated Ground Motion Prediction Equations (GMPEs) from the Next Generation Attenuation relationships (NGA west 2) (Bozorgnia et al. 2014) are adopted for the estimation of ground motion parameters at different seismogenic depths. A detailed comparison of this study with the earlier studies is listed in the Table 2.

Pakistan and its surroundings are situated on the boundary between the Indian, Eurasian, and Arabian tectonic plates. The seismo-tectonic environment of the region is shown in the Fig. 1. The Indian and Eurasian plates are in a state of very slow convergence spanning over 30 to 40 million years (Aitchison et al. 2007). This interaction has resulted in several mega-earthquakes, also evidenced by the seismicity of the last 100. In the north, the two plates are in a state of head-on collision with a slip rate of 37 to 42 mm/year (Chen et al. 2000). This has resulted in the formation of the Himalayan mountain ranges. The north-west Himalayan folds and thrust belt stretches from the eastern Kashmir basin to the western Afghan border near Parachinar. The NW Himalayan belt has several important thrust faults including the Main Boundary Thrust (MBT), Punjal Thrust (PT), Salt Range Thrust (SRT), the Himalayan Frontal Thrust (HFT), Hazara arc, and Himalaya arc.

The Hindukush and Pamir ranges situated in the north-west is the center for deep earthquakes. Both of these ranges are complex subduction zones (Negredo et al. 2007). The Pamir ranges extending from Hindukush ranges in the west through the Wakhan (Afghanistan), Chitral (Pakistan) to Kongur Tagh (China) in the east (Arnaud et al. 1993). Most of the part of Pamir range is located in Tajikistan (Central Asia). The Hindukush range stretches from Afghanistan to northern Pakistan and China (having a length of 800 km) and is the extension of Karakorum, Himalaya and Pamir mountain range (Searle and Mike 2013).

In the southwest, the oceanic floor of Oman (Arabian plate) subducts under the Eurasian plate, forming the Makran subduction zone (MSZ) (Stoneley 1974). The eastern margin of the Makran subduction zone is the left-lateral (sinistral) transform fault called the Ornach-Nal fault which is the southward extension of the Chaman fault (junction between the Eurasian and Indian plates). The Minab fault system (Zagros fold and thrust belt) in Iran forms the western margin of the Makran subduction zone (Regard et al. 2010). The Arabian and Eurasian plates are converging with a slip rate of 36.5 to 42 mm/year (DeMets et al. 1990). Recently, Ahmad et al. (2018) reported that the Arabian plate is moving towards the Eurasian plate with an average velocity of 23 mm/year at the Strait of Hormuz.

In the west, the fold and thrust belt includes the Sulaiman and Kirther belt which extends 600 km from Khuzdar city in the south towards the north. It then bends in the Quetta Syntaxes towards the southeast (Bannert and Raza 1992). The major sinistral strike-slip faults such as Chaman fault, Ghazaband fault, and Ornach-Nal faults also locate in this area. The slip rate of these sinistral strike-slip faults is approximately 30 mm/year (Khan et al. 2008). The faulting mechanisms of these faults is characterized by the translation and counterclockwise rotation of the Indian plate with respect to Eurasian plate along the whole length. The thrust faults such as Kohlu, Mekhtar and Ziarat are also located in the northern part of this fold and thrust range (Bannert and Raza 1992; Kazmi and Jan 1997).

Table 2 A comparison of this study with the past PSHA studies carried out for Pakistan and surrounding regions

Study	GSHAP (Zhang et al. 1999)	PMD and NORSAR (2007)	NESPAK (2007)	Zaman et al. (2012)	EMME (2014)	Current study
Year	1992–1999	2007	2007	2012	2014	2019
Methodology	PSHA using Cornell (1968) and (McGuire 1976) approach	PSHA using Cornell (1968) and (McGuire 1976) approach	PSHA using Cornell (1968) and (McGuire 1976) approach	National Seismic Hazard Maps (NSHM) using USGS Software for PSHA	Both Cornell (1968); McGuire (1976) and NSHM approaches with 60% and 40% probabilistic weights	Both Cornell (1968); McGuire (1976) and NSHM methods with 50% probabilistic weights assigned to each
Source models characterization	More than 20 seismic area sources with uniform seismicity	19 seismic area sources with uniform seismicity	17 seismic area sources with uniform seismicity	Background spatially smoothed-gridded seismicity	More than 18 seismic area sources with background spatially smoothed-gridded seismicity in two different source models	23 seismic area sources with background spatially smoothed-gridded seismicity in two different source models
Active crustal faults	Nil	Nil	28 active crustal faults modeled using characteristic fault model. The slip rate is not used to estimate the earthquake recurrence rate	13 active crustal faults modeled, using both the characteristic and Gutenberg-Richter (GR) models with equal weightage to estimate the earthquake recurrence rate	More than 100 active faults are modeled, using GR model by Anderson and Luco (1983) to estimate the earthquake recurrence rate	110 active crustal faults modeled using the GEM (2019) active faults catalogue. Both the characteristic and GR models by Youngs and Coppersmith (1985) with equal probabilistic weightage are used to estimate the earthquake recurrence rate

Table 2 (continued)

Study	GSHAP (Zhang et al. 1999)	PMD and NORSAR (2007)	NESPAK (2007)	Zaman et al. (2012)	EMME (2014)	Current study
Makran subduction zone	Modeled as simple area source	Modeled as simple area source	Modeled as simple area source	The interface between two tectonic plates is modeled as sloping area source	The inter slab seismicity (0–50 km) is modeled as complex inclined area source, whereas the in slab seismicity (50–150 km) is modeled as simple area source	The seismicity associated to the interface between two tectonic plates (5–55 km) is modeled as a complex sloping area source. Whereas the shallow (0–5 km) and deep in slab (55–250 km) seismicity is modeled as background seismicity
Earthquake catalogue	Pre-historic (before 1900) and historic (1900–1997) earthquake catalogue with $M_w > 5$	102 years (1905–2007) earthquake catalogue with $M_w > 4.8$	102 years (1904–2006) earthquake catalogue with $M_w > 4.5$	107 years (1902–2009) earthquake catalogue with $M_w > 4.5$	Pre-historic (before 1900) and historic (1900–2006) earthquake catalogue with $M_w > 4$	Pre-historic (before 1900) and historic (1900–2018) earthquake catalogue with $M_w > 4$

Table 2 (continued)

Study	GSHAP (Zhang et al. 1999)	PMD and NORSAR (2007)	NESPAK (2007)	Zaman et al. (2012)	EMME (2014)	Current study
Classification of Earthquake depth	Nil	Classify the seismicity of Hindukush region into shallow, intermediate and deep layers (0–30 km, 30–120 km and 120–300 km)	Nil	Classify the background seismicity into very shallow, shallow, intermediate and deep layer (0–25 km, 25–50 km, 50–100 km and 100–250 km) throughout the study area	Classify the background seismicity into shallow, in slab and deep layer (0–40 km, 40–100 km and > 100 km). Deep seismicity is considered only in Hindukush region. The in slab seismicity in subduction zone, whereas the remaining background seismicity is modeled using only shallow seismicity	Classify the background seismicity into very shallow, shallow, intermediate and deep layer (0–25 km, 25–50 km, 50–100 km and 100–250 km) for faults seismic source model, whereas for the area source model the BG seismicity is distributed into shallow (0–50 km) and deep (50–250) layers throughout the study area

Table 2 (continued)

Study	GSHAP (Zhang et al. 1999)	PMD and NORSAR (2007)	NESPAK (2007)	Zaman et al. (2012)	EMME (2014)	Current study
GMPEs	Only single GMPE of (Huo and Hu 1992) was used for ground motion estimation No multiple GMPEs were used to deal with the epistemic uncertainty	GMPE of (Ambraseys et al. 2005) was used Multiple GMPEs were not used to deal with the epistemic uncertainty	GMPE of (Boore et al. 1997) was used. Multiple GMPEs were not used to deal with the epistemic uncertainty	Multiple GMPEs for different earthquake environments were used For crustal faults, very shallow and shallow: three NGA west 1 GMPEs CB08(0.33), BA08(0.33), CY08(0.33) Intermediate: Y97(0.5), AB03(0.5) Deep: Y97(1.0) Subduction zone: Y97(0.25), AB03(0.25), Z06(0.5)	Multiple GMPEs for different earthquake environments were used Active shallow crustal region: AK14(0.35), CY08(0.35), AC10(0.2), Z06(0.1) Stable shallow crustal region: AB06(0.4), C03(0.25), T97(0.35) Deep Seismicity: Y97(0.5), LL08(0.5) Subduction zone: Z06(0.4), Y97(0.2), AB03(0.2), LL08(0.2)	Multiple GMPEs for different earthquake environments were used For crustal faults, very shallow and shallow: three NGA west 2 GMPEs CB14(0.33), BA11(0.33), CY14(0.33) Intermediate: Y97(0.5), AB03(0.5) Deep: Y97(1.0) Subduction zone: Y97(0.25), AB03(0.25), Z06(0.5)

Table 2 (continued)

Study	GSHAP (Zhang et al. 1999)	PMD and NORSAR (2007)	NESPAK (2007)	Zaman et al. (2012)	EMME (2014)	Current study
Results	PGA map for 10% PE in 50 years (475 years return period)	PGA and SA (0.2, 0.5, 1.0 and 2.0 s) values for return periods of 50, 100, 200, 500 and 1000 years Hazard curves and UHSs for major cities were developed	PGA map for 475 years return period PGA values for major cities are also given	Arithmetic mean PGA and SA (0.2, 1.0 s and 2.0 s) maps for return period of 475 and 2475 years Hazard curves were developed for major cities of Pakistan	Hazard results are reported in mean 5, 16, 50, 84 and 95% quartile ground motions. The PGA and SA (0.1, 0.15, 0.2, 0.25, 0.30, 0.50, 0.75, 1.0 and 2 s) maps are developed for return periods of 72, 475, 975, 2475 and 4975 years	Hazard results are presented in mean ground motion. The PGA and SA (0.2, 1.0 s and 2.0 s) maps are developed for return period of 475 and 2475 years Hazard curves and UHSs were developed for five major cities of Pakistan

CB08: Campbell and Bozorgnia (2008), BA08: Boore and Atkinson (2008), CY08: Chiou and Youngs (2008), CB14: Campbell and Bozorgnia (2014), BA11: Atkinson and Boore (2011), CY14: Chiou and Youngs (2014), Y97: Youngs et al. (1997), AB03: Atkinson and Boore (2003), Z06: Zhao et al. (2006), AK14: Akkar et al. (2014), AC10: Akkar and Çağnan (2010), AB06: Atkinson and Boore (2006), C03: Campbell (2003), T97: Toro (2002), LL08: Lin and Lee (2008) 2. Seismo-tectonic Environment of the Region

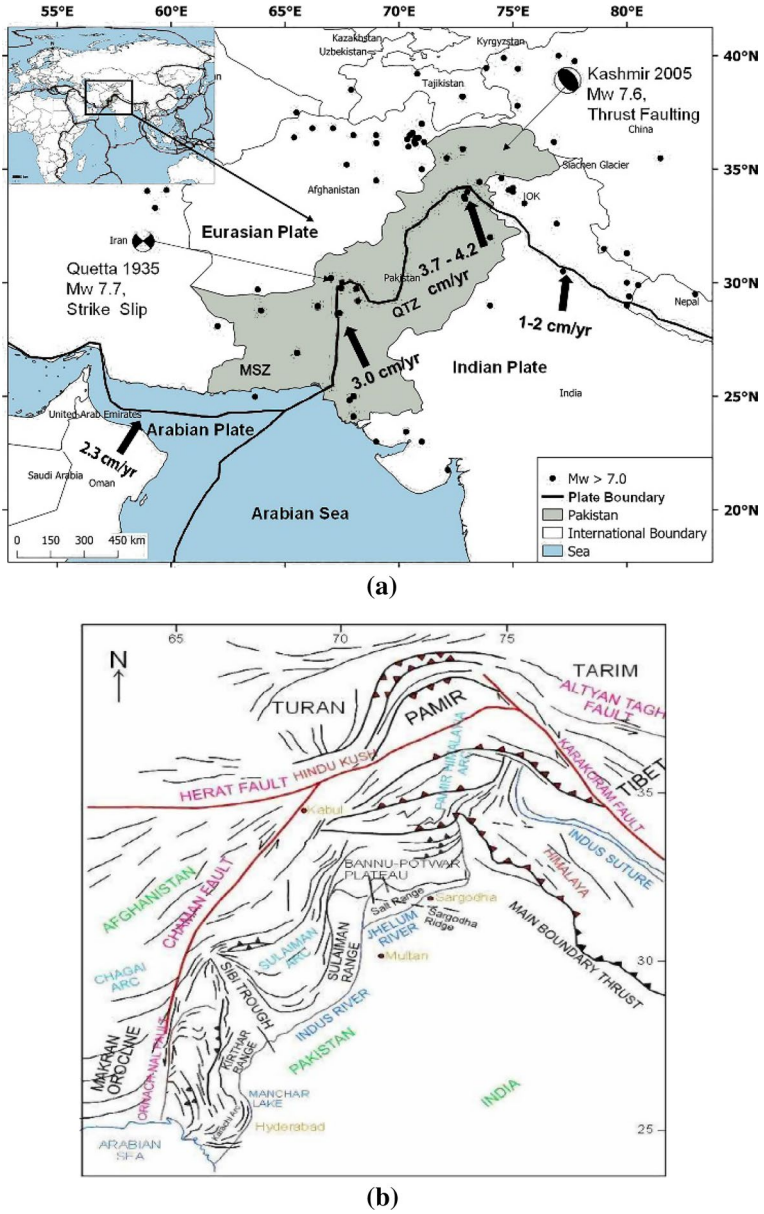

Fig. 1 The tectonic setting of Pakistan. Figure (**a**) shows the plate boundary between Indian, Eurasian and Arabian Plates with their respective slip rates. Figure (**b**) shows the tectonic features of the country (courtesy: Geological survey of Pakistan)

At the edge of the Sulaiman range (SR), the mountain range turn towards the west for approximately 300 km, which again take a sharp turn towards the south near Quetta (Rafi et al. 2012). This complex bent near Quetta is called the Quetta Transverse Zone (QTZ) as shown in the Fig. 1.

2 Earthquake catalogue

The information about the historical seismicity of a region is the prerequisite for the seismic hazard assessment. Therefore, it is necessary to compile a comprehensive database of past earthquakes in the form of a catalogue. The earthquake catalogue is used both for the seismic sources delineation and to determine the seismicity parameters (i.e. seismic activity rate, maximum magnitude etc.). In addition, the historical pattern (both spatial and temporal) of earthquake data provides a better understanding of the seismotectonics of an area.

In this study, an updated earthquake catalogue is developed by compiling the pre-historically reported (AD 10 to 1900 CE), historical (1900 CE to 1964 CE) and instrumentally recorded (1900 CE to December 2018 CE) earthquake events. The data for this compilation is obtained from several international and local databases. The international sources include South Asian Catalogue (SACAT), the International Seismological Center (ISC), National Earthquake Information Center (NEIC, USGS), National Geophysical Data Center (NGDC) and Global Centroid Moment Tensor (GCMT). The local sources include the Water & Power Development Authority (WAPDA) and the Pakistan Meteorological Department (PMD). The historical data were obtained from published literature (Ambraseys 2000; Ambraseys and Bilham 2014; Ambraseys and Douglas 2004; Khan et al. 2018; Quittmeyer and Jacob 1979; Zare et al. 2014). The earthquake events with epicenters located in the geographical coordinates of 20°– 40°N latitude and 58°– 83°E longitude are considered for the compilation of updated catalogue.

The international and national databases report the earthquake events in different magnitude scales. Therefore, the compiled catalogue contains various magnitude scales. For example, USGS and ISC frequently report events in 20-s surface-wave magnitude (M_S), short-period P-wave magnitude (mb), and moment magnitude (M_w), while PMD reports earthquake events in local magnitude (M_L), and GCMT catalogue commonly reports the events in moment magnitude scale (M_w). For this reason, it is required homogenizing the catalogue to a single representative magnitude scale. This study uses the moment magnitude as a representative scale. In order to homogenize the magnitudes, a set of magnitude conversion equations were developed by carrying out regression analyses for those events which were reported in two different magnitude scales including as shown in Table 3. These relationships are shown in Table 3. The duplicated events reported by more than one source are removed from the compiled catalogue. The events having identical year, month, day, hour, minute and having almost similar coordinates are considered as same/duplicated events. The time accuracy of the historical events (before 1900 CE) and early instrumental events cannot be guaranteed. Therefore, such events are carefully examined

Table 3 The homogenization relations between M_w and the other magnitude scales

Type of magnitude	Homogenization relation	Magnitude range	Number of paired events	R^2	Reference
M_w, mb	$M_w = 0.967mb + 0.1989$	$4.0 \le mb \le 6.2$	459	0.72	Current study
M_w, M_S	$M_w = 0.5396M_S + 2.7051$	$3.0 \le M_S \le 6.1$	728	0.70	Current study
	$M_w = 0.9336M_S + 0.3781$	$6.2 \le M_S \le 8.2$	76	0.73	
M_w, M_L	$M_L = M_w$	$M_L \le 6$	–	–	(Heaton et al. 1986)
M_w, M_D	$M_w = 0.764M_D + 1.379$	$3.7 \le M_D \le 6.0$	–	–	(Akkar et al. 2010)

manually for duplication by allowing the temporal margin. For historical events, having the same day of occurrence with same reported magnitude and location are considered as duplicated events. The number of events reduced from 71,759 to 34,104 after eliminating the duplicated events. A threshold magnitude of $M_w = 4.0$ is selected while compiling the catalogue. It is assumed that the events with magnitudes lower than this threshold may not provide any significant contribution towards the seismic hazard.

One of the fundamental assumptions of the PSHA methodology is the statistically independent occurrence of earthquake events (Poisson's assumption). Therefore, the mainshock events (independent events) are separated from foreshocks and aftershocks (statistically dependent events). This process of identifying and excluding the dependent events is known as declustering. In this study, the declustering algorithm developed by Gardner and Knopoff (1974) is used for this purpose. As a result of this process, the earthquake events in the catalogue were further reduced to 7,845, eliminating about 77% of the total events from the catalogue.

The difference between actual and the available recorded seismicity of the region is known as "incompleteness" (Rydelek and Sacks 1989). The earthquake catalogue should be as "complete" as possible for use in any seismic hazard analysis (Sawires et al. 2019). The completeness ranges vary for smaller magnitudes to the larger magnitudes. The completeness ranges for larger magnitudes are relatively wider extending back to the historical times as compared to the smaller magnitudes whose completeness ranges back to a few decades. The variation in the completeness is mainly related to the insufficiency and less sensitivity of the seismographs used in the past. There are several methods available in literature to measure the completeness of the earthquake catalogue. In this study, the completeness is analyzed by using two techniques; Visual Cumulative Method (CUVI) (Tinti and Mulargia 1985) and the Stepp (1973) method. The results from both methods yielded almost similar completeness ranges. These are listed in the Table 4. Figure 2 shows the time versus magnitude distribution of earthquake data with the completeness periods.

3 Modeling of seismic sources

To adequately represent the region's complicated seismicity environment, the first step is to model the active seismogenic sources. In this study, the seismic sources are characterized by two different and independent modeling approaches; (1) The conventional area source model and (2) the spatially smoothed gridded seismicity with active crustal faults model. The hazard results obtained from both these models are combined in a logic tree framework with 0.5 weights assigned to each model. The recently compiled active crustal faults

Table 4 The periods of completeness for the developed earthquake catalogue in this study

Magnitude class	Completeness period	Magnitude class	Completeness period
$M_w \geq 4.0$	1990–2018 = 28	$M_w \geq 6.5$	1900–2018 = 118
$M_w \geq 4.5$	1975–2018 = 43	$M_w \geq 7.0$	1900–2018 = 118
$M_w \geq 5.0$	1951–2018 = 67	$M_w \geq 7.5$	1884–2018 = 134
$M_w \geq 5.5$	1926–2018 = 92	$M_w \geq 8.0$	1878–2018 = 140
$M_w \geq 6.0$	1900–2018 = 118		

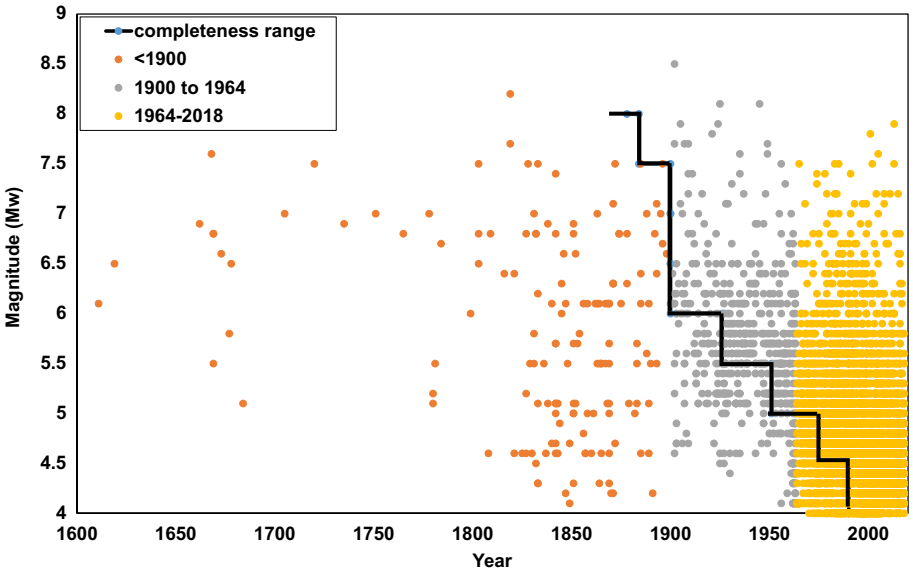

Fig. 2 The time versus magnitude distribution of earthquake data with the completeness periods

database (GEM 2019) is employed for the delineation and parameterization of the seismogenic sources. In order to ensure the consistency and continuity in the seismic hazard values, the active crustal faults in Pakistan and the neighboring countries within a buffer zone of 200 km are considered in this study.

3.1 Area sources model

The area sources are generally used to model the background seismicity of the region with mapped or unmapped faults. In this approach, the seismicity of the region is assumed to be uniform and homogeneous within a source zone. The area sources are generally delineated according to the historical seismicity pattern in a region. There are various studies which propose delineated area sources for Pakistan and surrounding regions (Danciu et al. 2018; Khan et al. 2018; PBC 2007; Rafi et al. 2012; Zhang et al. 1999). In this study, Pakistan and the surrounding areas are divided into 23 shallow crustal source zones (0–50 km) and 5 deep source zones (50–250 km), (Figs. 3 and 4). The delineation of area sources is performed by considering the seismicity pattern and active crustal faults of the region. The delineation of area sources performed in GSHAP (Giardini 1999) and EMME (Danciu et al. 2018) are also taken into consideration. The features of all area source delineations and their justifications in the previous studies were combined in order to get an insight in this process. The seismic hazard of the area is underestimated when large area sources are used instead of smaller area sources. The phenomena is called spatial smearing (Aki 1988). To avoid this phenomenon, relatively smaller area source zones are delineated in this study.

Generally, the magnitude frequency distribution (MFD) for the seismic area source zones is characterized by the standard Gutenberg-Richter (GR) law as given by the Eqs. (1) to (3). It encompasses the magnitudes of infinite length. In this study therefore, the MFD for the seismic area source zones is characterized by the truncated Gutenberg-Richter (GR) model as

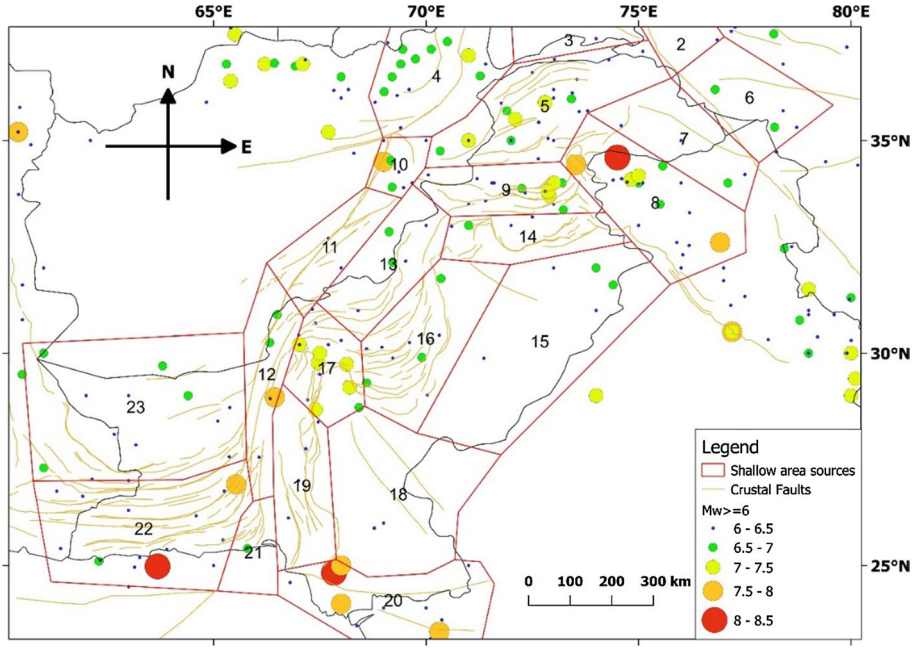

Fig. 3 Twenty-three Shallow seismic source zones delineated based on the crustal faults and historical seismicity with seismogenic depth less than 50 km

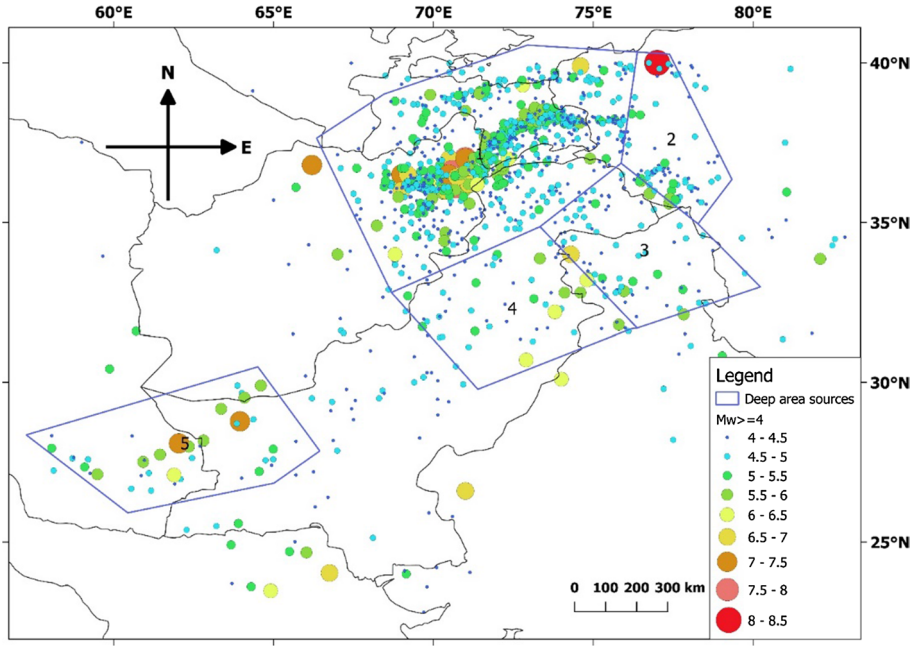

Fig. 4 Five deep seismic *source* zones shown by the blue polygons. These are delineated using the seismicity pattern of events having depth greater than 50 km

given by the Eq. (4) (Gutenberg and Richter 1956). The a and b values are the y-intercept and the negative slope of the Gutenberg-Richter magnitude frequency distribution curve. The seismicity parameters a and b show the seismic activity of shallow and deep area source zones. According to Aki (1965), the distribution of main shocks cannot be completely described by GR law. Consequently, it is not correct to use the GR exponential model to estimate the b value. Therefore, the maximum likelihood method proposed by Aki (1965) with the modifications of standard deviation error δb (Eq. 3) (Shi and Bolt 1982) is used to estimate the value of b (Eq. 2). The standard deviation error δb is not included in the model uncertainty. The seismicity parameters are estimated using the declustered catalogue within the completeness ranges and are shown in Table 5.

$$\log_{10} N(Mw) = a - bMw \tag{1}$$

Table 5 The seismicity parameters for 23 shallow and 5 deep sources used in the conventional area sources model

Zone	Events	a	b	D_{max}	M_{min}	M_{max}
Shallow seismic zones						
1	637	2.92	0.53	50	4	7.6
2	52	3.59	0.874	37	4	6.2
3	83	4.87	1.02	43	4	6.3
4	239	2.46	0.53	50	4	7.5
5	246	2.85	0.60	50	4	7.4
6	121	2.72	0.64	49	4	7
7	107	6.04	1.23	50	4	6.7
8	264	3.63	0.765	50	4	7.9
9	136	2.84	0.65	48.4	4	7.5
10	57	3.34	0.79	50	4	6.8
11	59	2.99	0.74	43	4.1	6.2
12	101	3.33	0.741	50	4.1	7.6
13	89	3.49	0.82	47.2	4	6.1
14	104	2.87	0.63	50	4	6.6
15	142	3.73	0.81	50	4	7
16	257	3.67	0.76	50	4	6.8
17	150	3.69	0.79	43	4	7.4
18	70	3.85	0.88	50	4	6
19	131	3.18	0.71	38.5	4	6.3
20	74	2.42	0.62	48	4	7.8
21	23	2.81	0.77	44.8	4.2	5.9
22	74	3.13	0.65	48	4	7.8
23	133	3.27	0.72	50	4	7
Deep seismic zones						
1	795	3.5	0.63	456	4	7.9
2	71	2.45	0.655	311	4	8.5
3	64	4.69	1.05	750.6	4	6.7
4	41	2.71	0.664	372	4	6.3
5	38	5.42	0.931	185.9	4.1	7.5

$$b = \frac{log_{10}e}{M - M_{min}} \tag{2}$$

$$\delta b = 2.3b^2 \sqrt{\frac{\sum(M_i - M)}{n(n-1)}} \tag{3}$$

where M is the average magnitude, M_i is the magnitude of the *ith* event, M_{min} is the minimum magnitude and n is the total number of events in the set. The mean annual rate of exceedance λ can be determined as follows.

$$\lambda = \nu_0 \frac{exp^{-\beta(M_w - M_w^{min})}}{1 - exp^{-\beta(M_w^{max} - M_w^{min})}} \tag{4}$$

where $\nu_0 = \exp(\alpha - \beta M_w^{inf})$, and M_w^{min} and M_w^{max} are the minimum and maximum magnitudes. It is assumed that the earthquake events with magnitude lower than M_w4 may not result in any significant damage to the structures. Therefore, M_w4 is selected as the lower bound magnitude (M_w^{min}). On the other hand, the maximum magnitude (M_w^{max}) in each area source is selected as the maximum observed magnitude plus 0.5. This margin of 0.5 is selected to account for any uncertainty in M_w^{max} estimation.

The seismicity parameters for each area source (Table 5) are calculated using the aforementioned GR model by employing the ZMAP (Wiemer 2001) software package. In shallow seismic sources, the observed variation of 'b' value is from 0.529 to 1.23, while in deep seismic sources the value of 'b' varies from 0.63 to 1.05. The seismic activity is higher for the seismic sources located in the north-western part of the country near the Hindukush region. Similarly, the area sources near southern Punjab and Sindh are seismically less active due to lower levels of historical seismicity.

3.2 Spatially smoothed seismicity with crustal faults model

The second source model used in this study is the spatially smoothed gridded seismicity model with crustal faults. In this model, the active crustal faults, background seismicity (spatially smoothed) and subduction zone are explicitly modeled. These are discussed separately as follows.

3.3 Modeling of the background seismicity

In order to avoid the subjectivity introduced due to conventional area source model, Frankel (1995) used a zone-free spatially smoothing approach for modelling the background seismicity. In the Frankel (1995) spatially smoothed seismicity approach, the seismicity rate is estimated by overlaying a grid of specified spacing (in this case $0.1° \times 0.1°$). The number of events having magnitude greater than M_{ref} (reference magnitude) are then counted in each cell for different magnitude intervals. The count represents the maximum likelihood estimate of 10^a for that particular cell. The grid of numbers is then spatially smoothened with a 2-dimensional Gaussian function with correlation distance (c) (Frankel 1995). The spatially smoothed value $\overline{n_i}$ is derived using the Frankel (1995) multivariate kernel distribution function as given in Eq. (5).

$$\overline{n_i} = \frac{\sum_j n_j e^{\frac{-\Delta_{ij}^2}{c^2}}}{\sum_j e^{\frac{-\Delta_{ij}^2}{c^2}}} \tag{5}$$

where $\overline{n_i}$ and n_j are the smoothed rate of seismicity in the i-th and j-th grid cell. Δ_{ij} is the center-to-center distance between i-th and j-th cells. The value c is the correlation distance within which the seismicity rate of a particular cell is influenced by the neighboring cells.

In this study, the spatially smoothed background seismicity model is used to represent the earthquake occurrence pattern of the region in the areas of unmapped faults, and in the buffer zones assumed on both sides of the crustal faults. Therefore, the background seismicity in this model is divided into two zones; (1) the unmapped fault zone and (2) the buffer zone around the active crustal faults. Also, the events having different seismogenic depths do not contribute equally to the seismic hazard of a particular site. Therefore, the background seismicity in each zone is again divided into four layers on the basis of their seismogenic depths, ranging from 0–25 km, 25–50 km, 50–100 km and 100–250 km. In order to avoid the duplication of earthquakes linked to the active crustal faults, the earthquake events in the buffer zones having $M_w < 6.5$ are assigned to the background seismicity in the buffer zone. Whereas the events having $\mathrm{M_w} \geq 6.5$ are assumed to be faults-specific (Petersen et al. 2008). The Frankel (1995) spatially smoothing algorithm is used to get the seismicity rates (10^a) at each point in a grid of spacing $0.1° \times 0.1°$ in the study region. Since there is no formal guideline available for the selection of correlation distance 'c' (Ornthammarath et al. 2011), different values of 'c' were tested for spatial smoothening. After a number of trials (20 km, 30 km, 40 km and 50 km), it was observed that by decreasing the value of 'c', the smoothed seismicity concentrates around the parent cells containing the cluster of events. Similarly, by increasing the value of 'c', the seismicity rate of each cell spreads out largely to the neighboring cells. Therefore, in order to preserve the overall pattern of historical seismicity in the study region, a correlation distance of 50 km is finally selected to smoothen the background seismicity. Figure 5 presents the background smoothed activity rates (10^a values) derived using the Frankel (1995) approach.

The spatially smoothed seismicity is then modeled using the point source model at the center of each grid cell. The geometrical (depth and style of faulting) and seismicity parameters (a, M_{max} and M_{min}) are assigned to each point source. For background seismicity (unmapped fault zone) the maximum magnitude of $M_{w,max}$ 7.4 is assigned, as this is the maximum magnitude observed in the unmapped fault zone. The seismic activity of unmapped fault zone is assumed to be lower than the mapped fault zone. While in the buffer zone $M_{w,max}$ 6.4 is assigned as the maximum magnitude to every point source. Earthquakes having $Mw \geq 6.5$ are assumed to be faults specific. The events having $M_w \geq 6.5$ were removed from the buffer zones of active crustal faults before the spatial smoothening. Events having magnitude greater than M_w 4 are used to assess the seismic hazard in the background, as the earthquake events with smaller magnitudes are having a very little effect on the structures (Bommer et al. 2001). The activity rate for the background seismicity is computed using the truncated Gutenberg Richter model (GR) (Eq. 1). The value of $b = 0.9$ is assumed to be uniform for modeling the background seismicity. The 'b' value is computed using the complete earthquake data within the boundary of the country. In contrast the value of 'a' varies from cell to cell in the region as shown in the Figs. 5, 6 and 7.

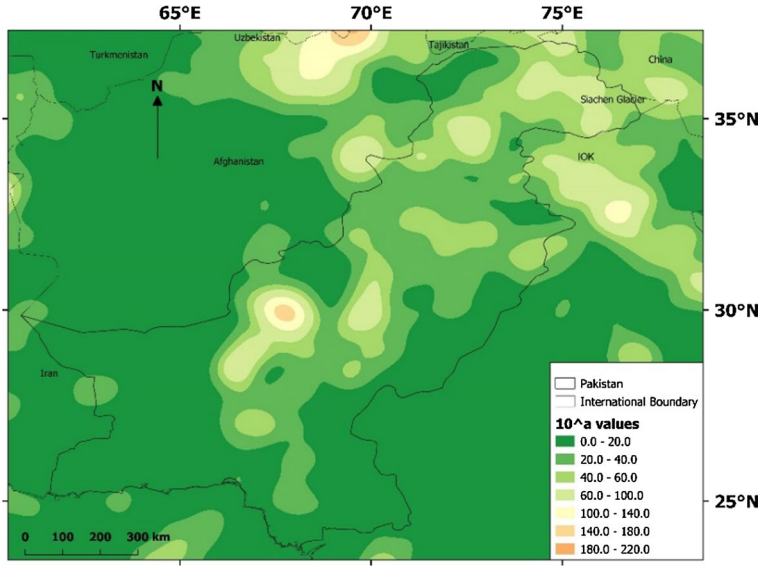

Fig. 5 The background smoothed activity rate 10^a values derived using Frankel (1995) approach

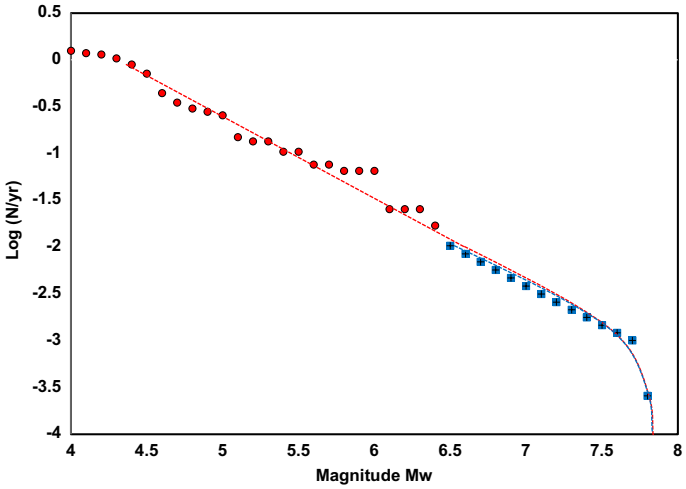

Fig. 6 The magnitude frequency distribution (MFD) for Zhob fault in Balochistan. The red line shows the Truncated Gutenberg-Richter MFD ($4 \leq M_w \leq 6.4$) using the earthquake events in the buffer zone of 15 km around the fault. The blue line shows the MFD ($M_w \geq 6.5$) of the Zhob fault calibrated from the slip rate using the Youngs and Coppersmith (1985) recurrence model

3.4 Modeling of crustal faults

The crustal faults data for Pakistan and surrounding areas are primarily obtained from the updated global active faults database of Global Earthquake Model (GEM 2019) and from the data reported by Kazmi and Jan (1997). A total of 110 active crustal faults in the administrative

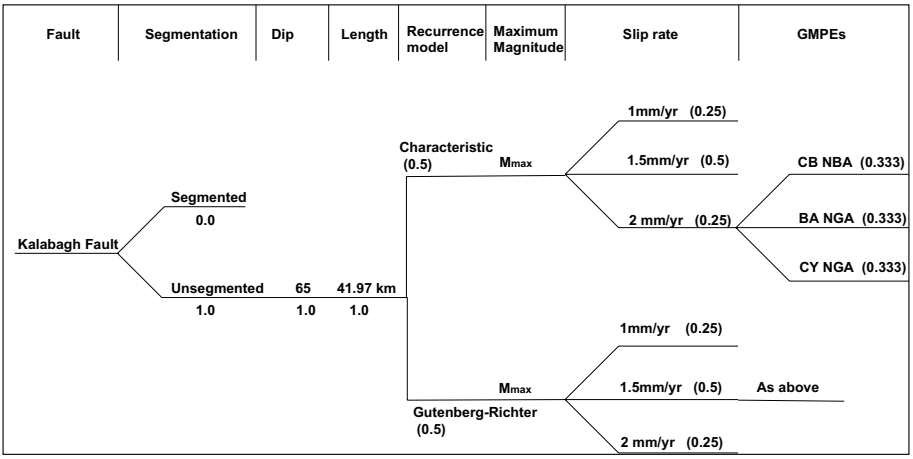

Fig. 7 The logic tree for Kalabagh fault *source* model used in the current study

boundary of Pakistan and the nearby areas (within 300 km) are incorporated and explicitly modeled as shown in the Fig. 8. The earthquake recurrence rate for higher magnitude earthquakes on crustal faults is determined by using the geometric parameters, faulting mechanism and geological slip rates of the crustal faults. A number of stochastic recurrence models i.e. (Anderson 1979; Anderson and Luco 1983; Stirling et al. 1996; Youngs and Coppersmith

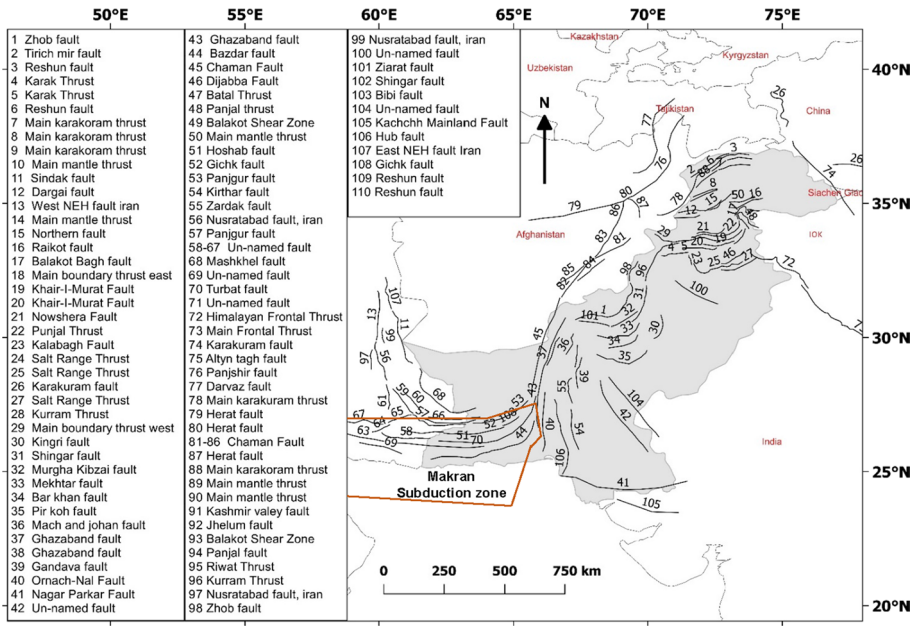

Fig. 8 Active crustal faults of Pakistan obtained from the GEM (2019) active crustal faults database and Kazmi and Jan (1997)

1985) are available to estimate the fault seismic activity from geological slip rates. In order to assess the earthquake recurrence rate of a fault from its geological slip rate, the seismic moment is first determined using the Eq. (6) (Fig. 9).

$$M_o = uLWs \tag{6}$$

where u is modulus of rigidity or shear modulus ($\sim 3 \times 10^{11}$ dyne/cm^2), and L, W and s are the rupture length, width and slip rate of the fault respectively. The relationship proposed by Hanks and Kanamori (1979) is used to convert the seismic moment into the earthquake magnitude, as given by Eq. (7).

$$LogM_o = cm + d \tag{7}$$

where c and d are constants ($c = 1.5$ and $d = 16.1$) known as the magnitude-moment scaling coefficients.

In this study, the magnitude-frequency distribution (MFD) models developed by Youngs and Coppersmith (1985) exponential (Eq. 7) and characteristic (Eq. 8) are used with an equal probabilistic weight of 50%. The important inputs for calculating the MFD of faults using the recurrence model include the fault-specific geometric parameters (Length and width), slip rate and the value of 'b'. The regional b value of 0.9 is estimated using the historical seismicity of the whole country. The value of $b = 0.9$ is kept constant for all faults. The Wells and Coppersmith (1994) empirical relationship is used for characterizing the maximum magnitude of faults using the faults geometry. The epistemic uncertainty related to maximum magnitude is not considered. The characteristic model used in this study is given by Eqs. (8) to (10) below.

$$\mu AS = b\dot{N}\left(m^0\right)M_0^{\mu}\exp\left(-\beta\left(m^{\mu} - m^0\right)\right)/(c-b)(1-\exp(-\beta(m^{\mu} - m^0))) \tag{8}$$

$$\mu AS = \frac{\left(\dot{N}\left(m^0\right) - \dot{N}(m^c)\right)\exp\left(-\beta\left(m^{\mu} - m^0 - 1/2\right)\right)M_0^{\mu}}{\left(1 - \exp\left(-\beta\left(m^{\mu} - m^0 - 1/2\right)\right)\right)} \cdot \left[\frac{b10^{-\frac{c}{2}}}{c-b} + \frac{b\exp(\beta)\left(1 - 10^{-\frac{c}{2}}\right)}{c}\right] \tag{9}$$

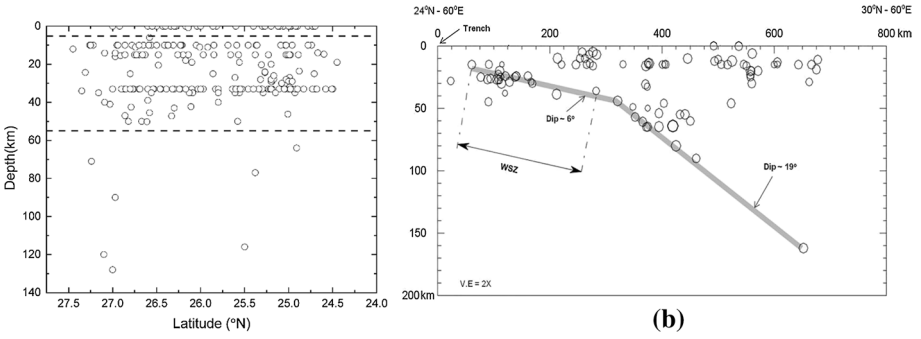

Fig. 9 The cross sections of the Makran subduction zone (**a**) Cross section through the MSZ along longitude 57°E covering the historical events from 57°E to 66°E and latitude between 24°N and 27.5°N. The figure shows most of the events are having depths between 5 and 55 km. (**b**) Cross section along longitude 62°E through the MSZ, including events from longitudes 58°E and 66°E and between latitude 24°N and 30°N, using the EHB catalogue up to 2004. The thick gray line shows the interface between the Eurasian and Arabian plates (modified from Aldama Bustos (2009))

$$\dot{N}(m^c) = \frac{b\ln(10)(\dot{N}(m^0) - \dot{N}(m^c))\exp(-\beta(m^u - m^0 - 3/2))}{2(1 - \exp(-\beta(m^u - m^0 - 1/2)))} \quad (10)$$

where $\dot{N}(m^0)$ and $\dot{N}(m^c)$ are the cumulative number of earthquakes having magnitude greater than the reference magnitude m^0 and characteristic magnitude m^c. M_0^u is the moment corresponding to the maximum magnitude m^u. A detailed discussion about the recurrence models can be seen in Youngs and Coppersmith (1985).

In order to avoid the double-counting of the earthquake events in background seismicity and active faults, a threshold magnitude of M_w 6.5 (also used by ESHM13 and Petersen et al. (2008)) is selected to separate the events associated to the background seismicity from those of the active faults. A symmetric buffer zone (15 km) is created on both sides of the active crustal faults. The earthquake events with magnitudes smaller than M_w 6.5 are assumed to have occurred in the background buffer zone, whereas the events larger than M_w 6.5 are assumed to be fault-specific. A verification of the consistency of two models (a) the background seismicity in the buffer zone, and (b) the crustal faults (calibrated from slip rates) is performed by comparing their occurrence rates. Figure 6 shows a comparison of the magnitude frequency distributions of both models for an example fault (Zhob fault in Balochistan). It can be seen that the magnitude frequency distribution (MFD) for the background seismicity in the buffer zone of 15 km around the faults (having $4 \leq M_w \leq 6.4$) is closely compatible with the fault's MFD ($M_w \geq 6.5$) calibrated from its slip rate (determined using the Youngs and Coppersmith (1985) recurrence model. The important parameters of all the crustal faults (110 active faults) used in the study are listed in Table 7 in the Appendix. An example logic tree used for the crustal faults (e.g. for the Kalabagh fault source model) is shown in the Fig. 7.

3.5 Modeling of Makran subduction zone (MSZ)

The historical data for Makran subduction zone shows an intermediate to low seismicity except a few large magnitude earthquakes. The 1945 earthquake (M_w 8.2) is the maximum earthquake observed in this region. This event also generated a tsunami. In this region, the Arabian plate is subducting under the Eurasian plate with a dip angle of 10 degrees extending 400–500 km towards the north (Byrne et al. 1992). The annual subduction rate of the Makran subduction zone (MSZ) is approximately 32 to 35 mm/year (McClusky et al. 2003) on the eastern side. While at the western side between Iran and Oman, the convergence rate is 19.5 mm/years (Musson 2009). Figure 9 shows the north–south cross-section of the Makran subduction zone (MSZ).

In this study, the earthquake events in the subduction zone are divided into very shallow (0-5 km), shallow (5-55 km), intermediate (55-100 km) and deep (100-250 km). The activity of the Makran subduction zone is modeled using three types of seismogenic source models. (1) The faults and folds appearing on the upper surface of the subduction zone, (2) The shallow seismicity (5-55 km) is modeled as complex inclined area source zone and (3) the very shallow, intermediate and deep earthquakes are modeled as spatially smoothed seismicity similar to the aforementioned background seismicity. The earthquakes having a depth ranging from 5 to 55 km are assumed to have occurred on the interface of plates. To characterize the seismicity of the complex area source, the Gutenberg-Richter (GR) magnitude recurrence model (Gutenberg and Richter 1944) is used with M_w 8.2 as maximum magnitude M_{max}.

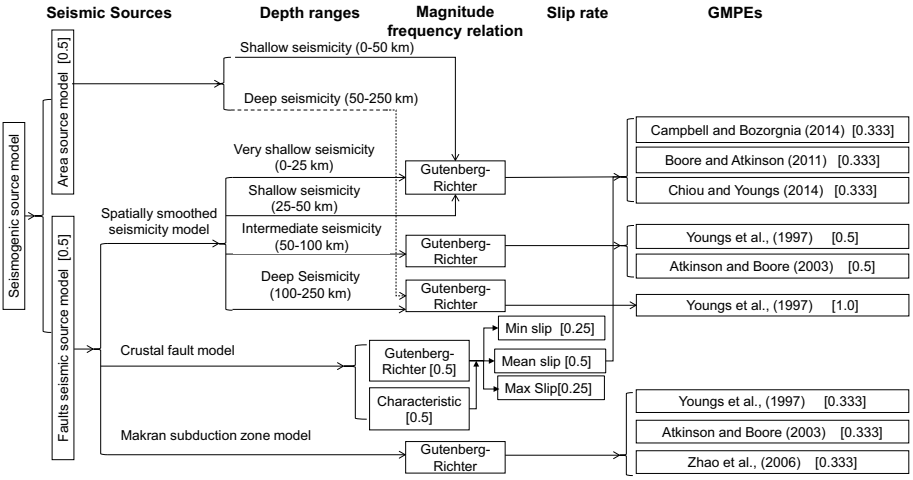

Fig. 10 The overall logic tree used for the seismic *source* model and GMPEs for performing the PSHA. The values in brackets show the probability weights for GMPEs

4 Ground motion prediction equations (GMPEs)

The GMPEs are used for the estimation of ground motion parameters i.e. peak ground accelerations (PGA) and spectral accelerations (SA) at various time periods. The source-to-site distance and earthquake magnitude are the key inputs to estimate the ground motions using GMPEs. Generally, the GMPE for a region is developed using the statistical regression analysis using the recorded data of strong ground motions. For Pakistan and surrounding region, very few recorded strong ground motions are available. Therefore, no GMPE is explicitly developed using the data specific to this region. Due to this limitation, the GMPEs developed for regions with similar tectonic environments are used in this study (Ornthammarath et al. 2011; Rafi et al. 2012; Zaman et al. 2012).

In the current study, multiple GMPEs are selected for each seismogenic source. The Next Generation Attenuation models (NGA west 2) (Bozorgnia et al. 2014) are used for very shallow (0–25 km), shallow (25–50 km) and crustal faults in the area. These GMPEs are Campbell and Bozorgnia (2014), Atkinson and Boore (2011) and Chiou and Youngs (2014). They are developed for the western US and estimate the ground motions for shallow crustal earthquakes in terms of PGA and SA (0–10 s) with 5% damping ratio. These GMPEs are considered suitable as the seismotectonic environment of study region is similar to the western US with tectonic features including converging plate boundaries and several shallow crustal active faults. An equal weightage of 0.333 is assigned to each of these GMPEs. To estimate the ground motions for earthquakes in the intermediate (50–100 km) and deep (100–250 km) layers, the GMPEs developed by Youngs et al. (1997) and Atkinson and Boore (2003) are selected in this study. Youngs et al. (1997) is used for earthquakes having depth ranging from 50 to 250 km, whereas Atkinson and Boore (2003) is used only for intermediate (50–100 km) seismicity. For the Makran subduction zone (MSZ), the ground motions for subduction interface is calculated using three GMPEs developed by Atkinson and Boore (2003), Youngs et al. (1997) and Zhao et al. (2006). Each GMPE is assigned with a probability weight of 0.333. The GMPEs selected and used

in this study represent an updated data and understanding of the ground motions in their regions (Petersen et al. 2008).

5 Probabilistic seismic hazard assessment and results

The seismic hazard assessment procedure includes various uncertainties and assumptions at each step. To minimize these uncertainties, the logic tree procedure proposed by Kulkarni et al. (1984) is adopted in this study. Generally, there are two types of uncertainties involved in estimating the ground motions; the epistemic and aleatory uncertainties. Aleatory uncertainty is the spatial uncertainty of earthquake occurrence in space and time window (when and where), for example, the magnitude and distance of any future event at a site. These types of uncertainties are accounted in the PSHA calculations using the integration procedure. The epistemic uncertainty, on the other hand, is caused by the lack of information and understanding of the geological processes, for example the unavailability of ground motion records for developing the attenuation model for a region. These types of uncertainties can be minimized by using different logic tree models with a certain probabilistic weightage assigned to each calculation path. In this study, this approach is used to account for the epistemic uncertainty in source models and various GMPEs for each tectonic region.

Figure 10 presents the overall logic tree used for the seismic source models and GMPEs for performing the PSHA. In order to account for the epistemic uncertainty in source modeling (at the first level of logic tree), an equal weightage (of 0.5 each) are assigned to both source models (i.e. the area source model, and the spatially smoothed seismicity model with crustal faults). At the second stage, the characteristic and exponential recurrence relationships for crustal faults are combined with 0.5 weightage assigned to each. At the third stage, the fault slip rates are included with 0.25, 0.5 and 0.25 weights for minimum, mean and maximum slip rates, respectively. At the fourth level, various GMPEs used for each seismic source type are combined according to their weights shown in Fig. 10.

The analysis is performed using the OpenQuake engine (Pagani et al. 2014). The hazard library of OpenQuake is a complete package for seismic hazard assessment. It allows the user to model the seismicity of the region through various types of seismic sources including simple and complex faults, and spatially smoothed gridded seismicity using (Frankel 1995) approach. This analysis platform is also equipped with a comprehensive library of GMPEs as well as the automated logic tree framework. In this study, a grid spacing of $0.1° \times 0.1°$(approximately 11 km) is used in both directions. At this grid spacing, the hazard calculations are performed at a total of 54,333 points in the study region. The hazard maps and hazard curves for the mean PGA and SA (0.2 s, 1 s and 2 s time periods) are developed for 2% and 10% probability of exceedance (PE) in 50 years exposure (corresponding to 2475 and 475 years return period) with 5% critical damping ratio. The hazard maps are produced for a standard reference site condition having a mean shear wave velocity of 760 m/s in the top 30 m of the crust. This reference site class corresponds to a boundary between site class B and C as prescribed by the National Earthquake Hazard Reduction Program (NEHRP).

Figure 11 presents the hazard maps of the study region for the mean PGA and SA (0.2 s, 1 s and 2 s time periods) at 2% and 10% probabilities of exceedance (PE) in 50 years exposure. The variation in hazard values for 10% PE in 50 years mostly follow the historical earthquakes pattern of the region as shown in the hazard maps for a specific hazard

parameter. The hazard values are higher around the major crustal faults near the main converging plate boundary. The effect is pronounced in the hazard maps for 2475 years return period (2% PE in 50 years). The PGA values in the study region vary from 0.1 to 0.7 g for 10% PE in 50 years, and 0.15 to 1.2 g for 2% PE in 50 years. The PGA values for 2475 years return period are 1.54 to 2.8 times greater than those for 475 years return period. The MCE-to-DBE PGA ratios are calculated for several major cities. For the cities of Quetta, Karachi, Peshawar, Islamabad and Lahore, this ratio is 1.61, 1.72, 1.64, 1.71, 1.62 and 1.69, respectively.

It can be seen that the hazard values are relatively higher in the northern and western parts of Pakistan. In north, the cities of Chitral, Gilgit, Swat, Dir, Kohistan, Mansehra, Abbotabad, Mirpur, Muzaffarabad, Neelam and Bagh have high seismic hazard mainly contributed by shallow and deep seismic sources in Hindukush, Pamir and Karakorum ranges. In the western part of Pakistan, the cities of Quetta, Ziarat, Mastung, Chaman and Sibi have higher hazard values mainly contributed by the strike slipping faults (e.g. Chaman fault and Ghazaband fault). In the southwestern Pakistan, the cities of Gawadar, Kharan and Panjgur have the higher hazard values mainly governed by the Makran Subduction Zone. The eastern Pakistan (e.g. the southern part of Punjab province) can be identified as a region with comparatively lower seismic hazard. Some of the active crustal faults e.g. the Himalayan frontal thrust, main boundary thrust, Jehlum fault and Riwat fault have the potential of producing large earthquakes close to major cities including the capital city of Islamabad, Rawalpindi and few areas of Azad Kashmir region.

A comparison of the PGA hazard maps (for 10% probability of exceedance in 50 years) developed in this study with those of previous studies is shown in the .

Figure 12 In the current study, the PGA values for major cities are significantly higher as compared to the previous studies. The pattern of hazard variation however is similar to those of the previous studies. The variations in the seismic hazard values for a specific site reported by different studies are of significant relevance in the structural design practice. Therefore, a comparison of PGA and SA values (for 475 years return period) between the current study with the previous studies (PBC 2007; Rafi et al. 2012; Şeşetyan et al. 2018; Zaman et al. 2012; Zhang et al. 1999) is presented in the Table 6 for major cities of Pakistan

The difference in estimated hazard values between the current study and previous studies can be attributed to several reasons. The methodology adopted in this study is mostly similar to the approaches used in the development of US national seismic hazard maps (NSHM) and in the EMME (2014). However, there are several updates in input datasets as well as differences at various steps of the analysis. For example, in the EMME (2014), the earthquake catalogue used in the analysis of this region was developed by Zare et al. (2014). This catalogue includes the earthquake events up to 2006 CE. Whereas in this study, an updated earthquake catalogue is compiled by including the events until 2018 CE. In this catalogue, an additional 1987 earthquake events are included with $M_w > 4$ occurred between 2006 and 2018 CE. Similarly, several local and international sources are consulted to make the developed catalogue more complete and reliable. Similarly, for combining the results from different source models, the EMME study considered a weightage of 60% and 40% for area source model and fault source model, respectively. Moreover, the deep seismicity is modeled using only deep area sources in both models. However, in the current study, it is assumed that an equal weightage (of 50% each) is more adequate to combine both the models. Also, the deep seismicity in current study is modeled in four layers (very shallow, shallow, intermediate and deep) in the fault source model. The modeling approach used for the Makran subduction zone (MSZ) and the selection of GMPEs is also among the

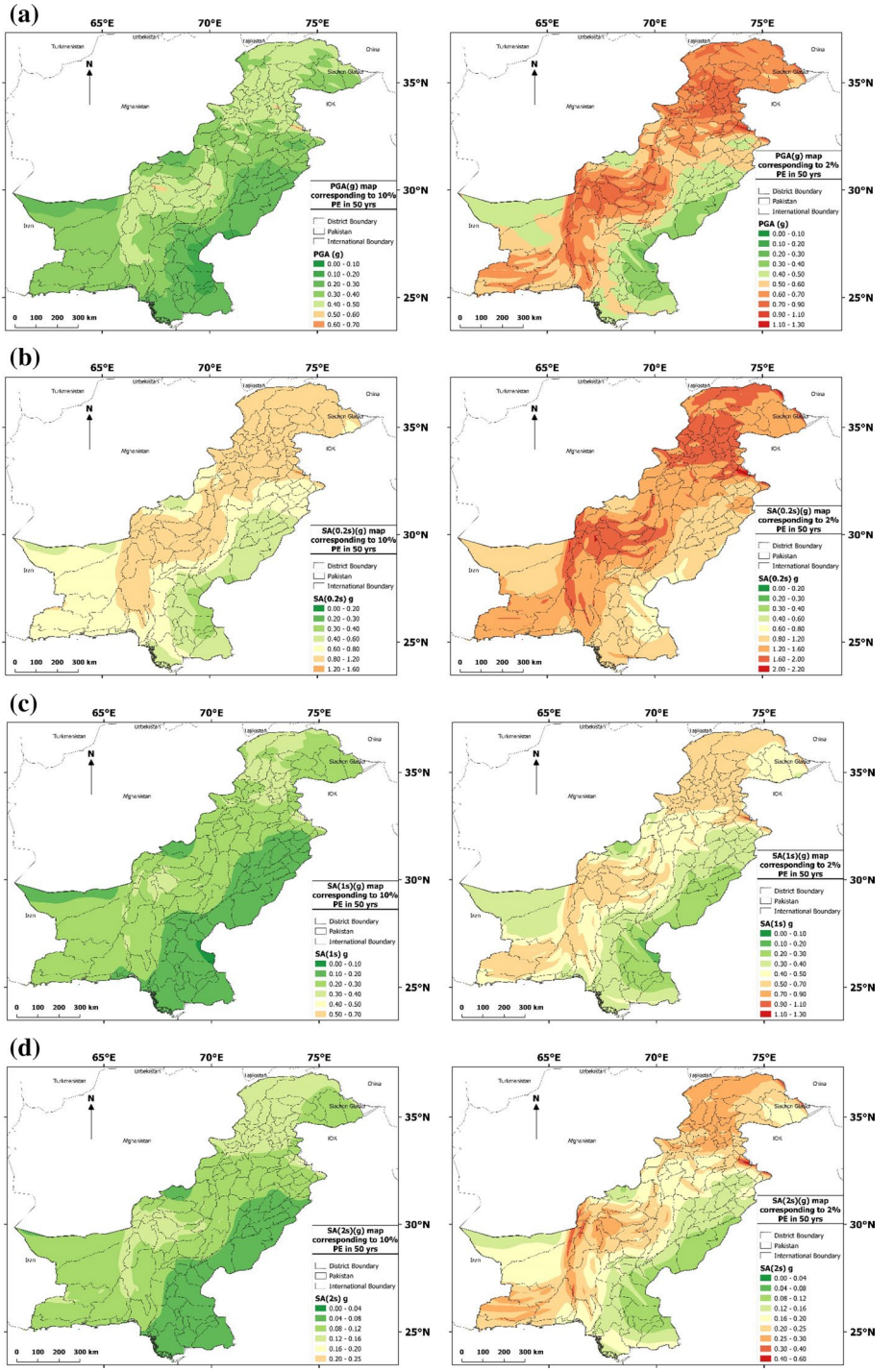

Fig. 11 The hazard maps for (**a**) PGA, (**b**) SA(0.2 s), (**c**) SA(1 s) and (**d**) SA(2 s) corresponding to 10% (475 years RP) and 2% (2475 years RP) probability of exceedance in 50 years

Fig. 12 Comparison of the seismic hazard maps of Pakistan for 10% PE in 50 year (475 year RP) (**a**) EMME (2014) (**b**) GSHAP (**c**) NESPAK (BCP 2007) (**d**) PMD and NORSAR (**e**) Zaman (2012) (left) and current study (Right)

several differences between the current study and previous studies. We believe that these methodological updates combined with improved input datasets resulted in a clearer and more reliable picture of the seismic hazard of the study region.

In addition to the hazard maps, the uniform hazard spectra (UHS) for return periods of 475 years and 2475 years are also developed for five major cities of Pakistan and are shown in Fig. 13. In order to account for the variation of seismic hazard within each city, a maximum and minimum UHS is also presented. The Fig. 14 presents the hazard curves of the study region for the mean PGA and SA (0.2 s, 1 s and 2 s time periods) at 2% and 10% probabilities of exceedance (PE) in 50 years exposure. Using these curves, the hazard parameters for any return period (or the probability of exceedance in certain exposure period) can be obtained and used in the performance-based seismic assessment of new and existing structures in the study region.

The presented PSHA results and maps can be used for the determination of hazard levels of sites in the study region for structural analysis and design purpose. The practicing structural designers can effectively use these results to mitigate the seismic risk by devising earthquake resistant design of infrastructural facilities. They can also be used by the disaster management authorities and building regulation agencies to devise effective disaster preparedness, mitigation, emergency preparedness and management strategies. The results can also be used as a basis for making effective disaster risk reduction policies in the country.

6 Conclusions

This paper presents an updated seismic hazard assessment of Pakistan and the surrounding region. In this assessment, the approaches adopted for the National Seismic Hazard Maps (NSHM) of US and the Earthquake Model for Middle East (EMME) are used to develop the hazard maps and curves at bedrock level. Compared to the previous studies, several improvements have been made at each step of the PSHA methodology to determine an updated and reliable set of hazard parameters in the country. The logic tree procedure is adopted to account for the epistemic uncertainties in the seismic source modeling and GMPEs. An updated earthquake catalogue is developed for modeling the historical background seismicity. The crustal faults were also modeled using the slip rates obtained from the database maintained by the Global Earthquake Model (GEM 2019). The PSHA is performed by combining two types of seismic source models i.e. (a) the conventional area sources model and, (b) the spatially smoothed seismicity with active faults model. The hazard maps are developed for PGA and SA at a period of 0.2, 1 and 2 s for 2% and 10% probability of exceedance in 50 years (return periods of 2475 and 475 years). It is noticed that the seismic hazard in Pakistan varies from low to very high with the PGA values varying from 0.1 to 0.7 g for the DBE level and 0.15 to 1.20 g for the MCE level. The hazard is significantly higher in northern and southwestern regions of the country which are closer to the main plate boundary, major active faults and the Makran subduction zone (MSZ). The hazard maps show that the pattern of hazard variation in the country is similar to several previous studies

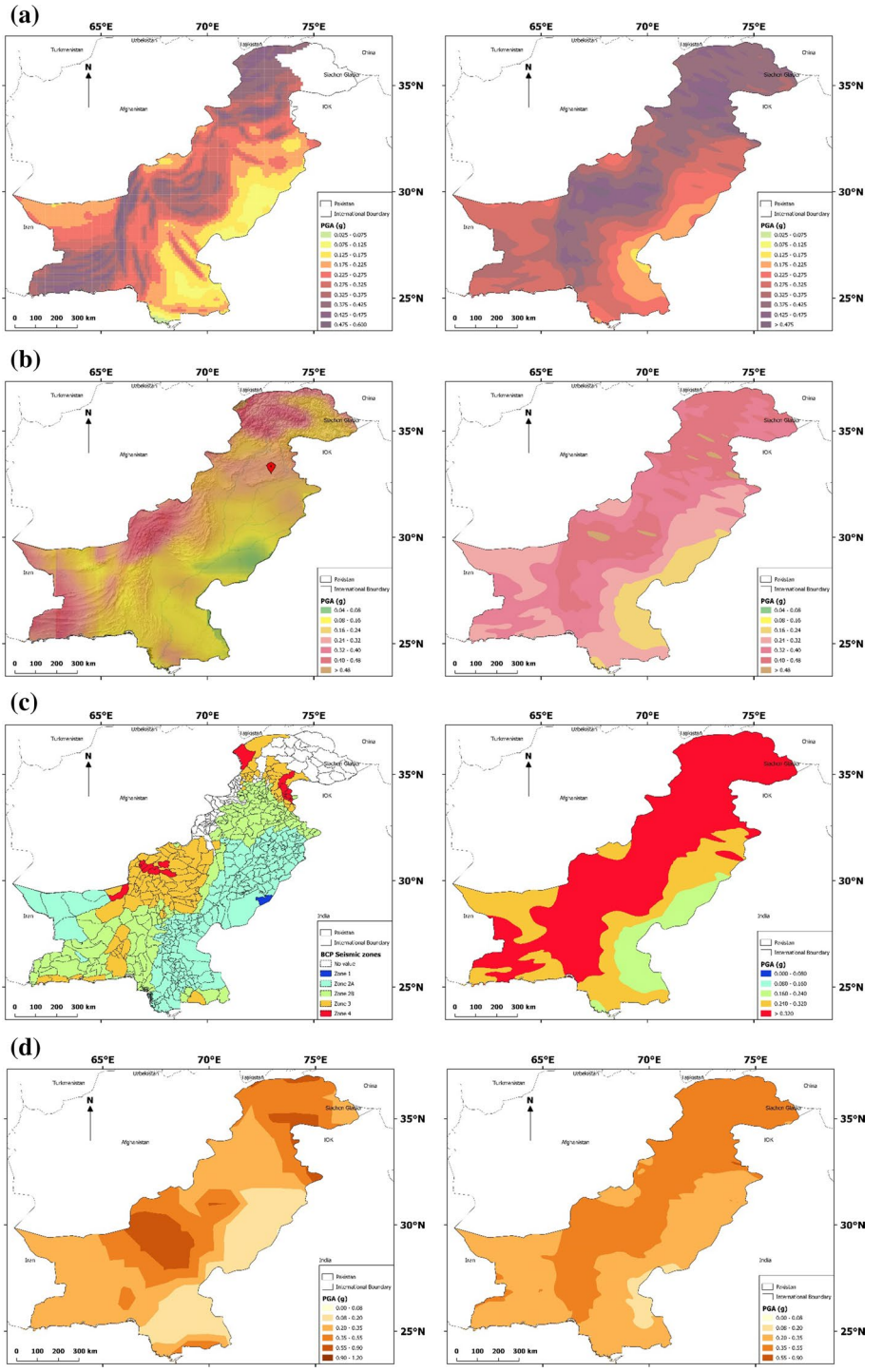
(a)
(b)
(c)
(d)
65°E
70°E
75°E
35°N
30°N
25°N
Turkmenistan
Uzbekistan
Tajikistan
China
Afghanistan
Iran
India
Siachen Glacier
IOK
N
0 100 200 300 km
Pakistan
International Boundary
PGA (g)
0.025 - 0.075
0.075 - 0.125
0.125 - 0.175
0.175 - 0.225
0.225 - 0.275
0.275 - 0.325
0.325 - 0.375
0.375 - 0.425
0.425 - 0.475
0.475 - 0.600
> 0.475
0.04 - 0.08
0.08 - 0.16
0.16 - 0.24
0.24 - 0.32
0.32 - 0.40
0.40 - 0.48
> 0.48
BCP Seismic zones
No value
Zone 1
Zone 2A
Zone 2B
Zone 3
Zone 4
0.000 - 0.080
0.080 - 0.160
0.160 - 0.240
0.240 - 0.320
> 0.320
0.00 - 0.08
0.08 - 0.20
0.20 - 0.35
0.35 - 0.55
0.55 - 0.90
0.90 - 1.20

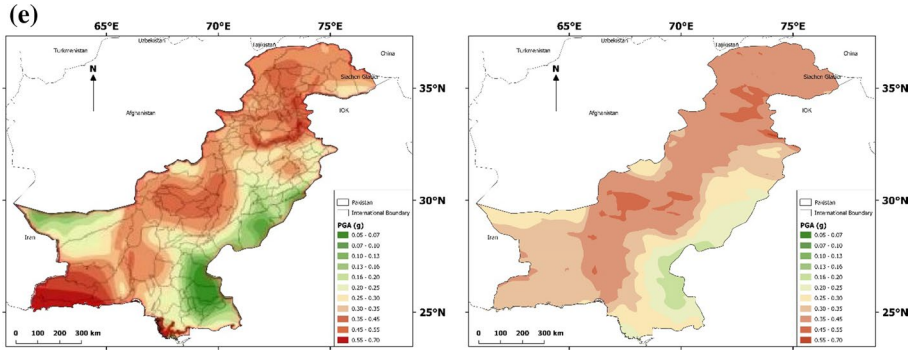

Fig. 12 (continued)

Table 6 The comparison of PGA and SA values (for 10% PE in 50 years) for major cities of Pakistan

Ground Motion Parameter	GSHAP (Zhang et al. 1999)	PMD and NORSAR (2007)	NESPAK (2007)	Zaman (2012)	EMME (2014)	Current Study
Islamabad						
PGA	0.32	0.37	0.24	0.45	0.44	0.446
SA (0.2 s)	–	0.57	–	1.01	0.99	1.02
SA (1.0 s)	–	0.14	–	0.26	0.23	0.30
SA (2.0 s)	–	0.08	–	0.10	0.13	0.13
Peshawar						
PGA	0.32	0.36	0.24	0.39	0.33	0.41
SA (0.2 s)	–	0.62	–	0.81	0.70	0.92
SA (1.0 s)	–	0.15	–	0.22	0.20	0.29
SA (2.0 s)	–	0.08	–	0.09	0.09	0.12
Quetta						
PGA	0.4	0.39	0.32	0.45	0.30	0.35
SA (0.2 s)	–	1.61	–	0.99	0.65	0.79
SA (1.0 s)	–	0.45	–	0.26	0.18	0.24
SA (2.0 s)	–	0.22	–	0.10	0.08	0.10
Karachi						
PGA	0.12	0.14	0.24	0.29	0.22	0.3
SA (0.2 s)	–	0.36	–	0.61	0.47	0.65
SA (1.0 s)	–	0.11	–	0.17	0.13	0.19
SA (2.0 s)	–	0.06	–	0.07	0.06	0.08
Lahore						
PGA	0.20	0.25	0.16	0.29	0.18	0.29
SA (0.2 s)	–	–	–	0.60	0.39	0.62
SA (1.0 s)	–	–	–	0.15	0.10	0.19
SA (2.0 s)	–	–	–	0.05	0.04	0.08

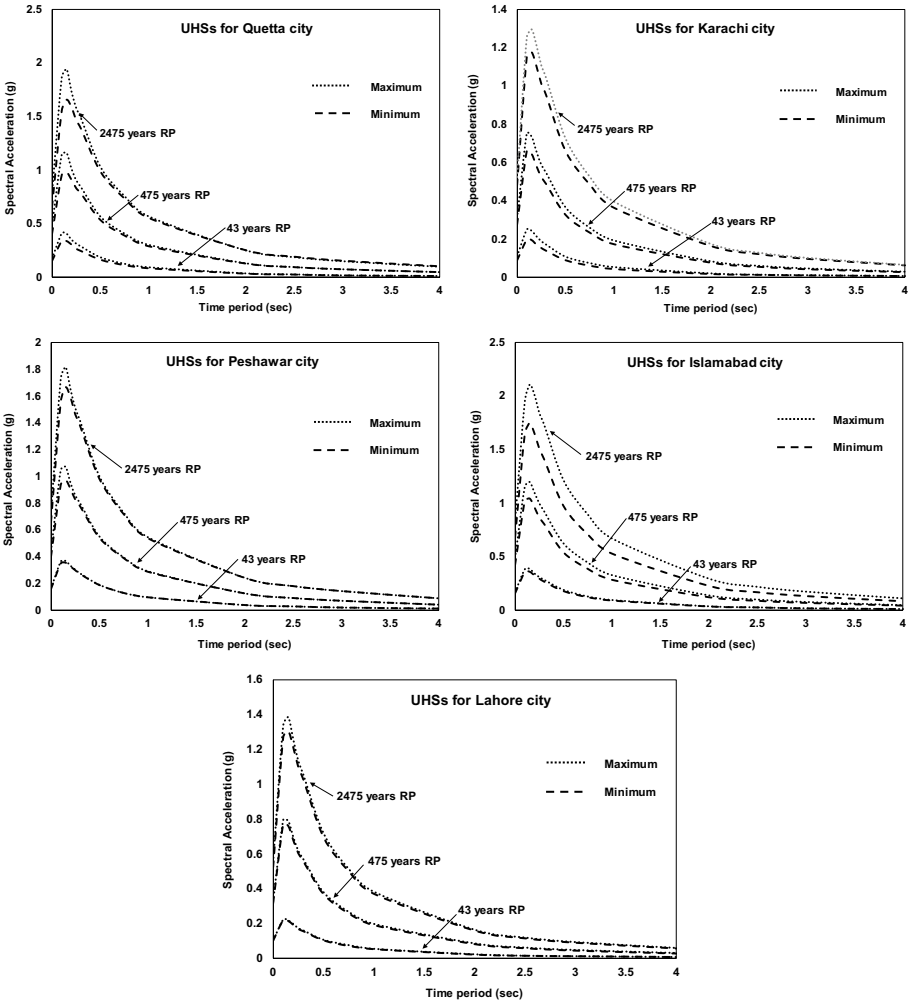

Fig. 13 Uniform Hazard Spectra (UHS) for 43 years, 475 years and 2475 years return periods for major cities (Peshawar, Islamabad, Lahore, Quetta and Karachi). The variation of uniform hazard spectra with in the city is shown by the maximum and minimum limits of the spectra

(PBC 2007; Rafi et al. 2012; Şeşetyan et al. 2018; Zaman et al. 2012; Zhang et al. 1999), however, the PGA and SA values are higher in varying degrees (except PMD and NORSAR 2007). The hazard curves and uniform hazard spectra for major cities of the country are also presented. These results provide an improved understanding of seismic hazard in Pakistan. They can be effectively used for the structural design and performance assessment of new and existing structures in the country. They may also be used as the basis for developing the improved strategies for the disaster risk reduction in the country.

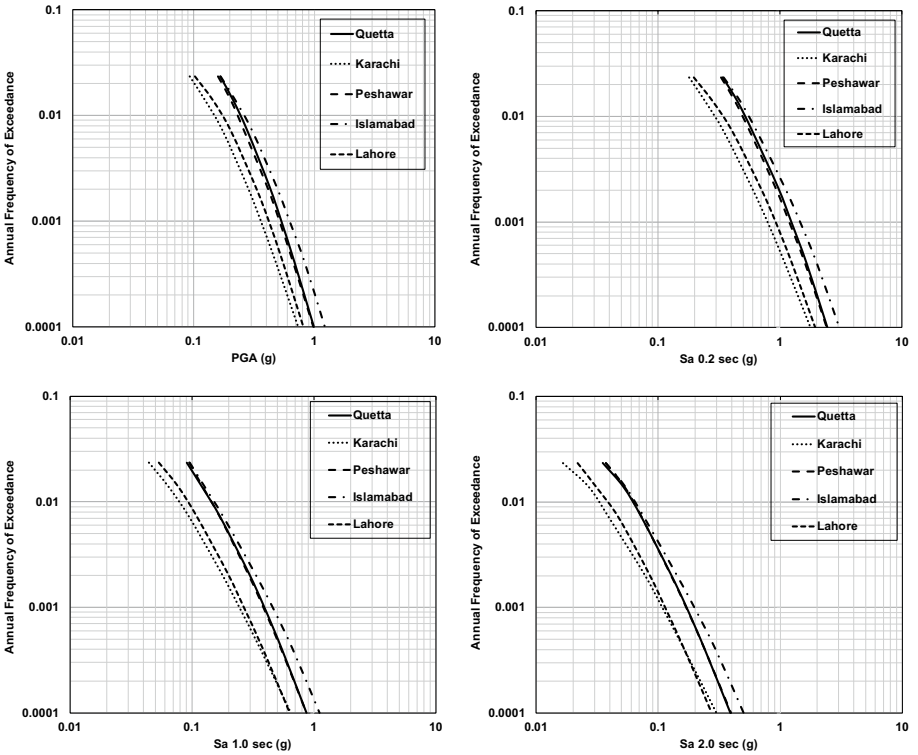

Fig. 14 The seismic hazard curves for PGA, SA (0.2 s), SA (1 s) and SA (2 s) for five major cities (Quetta, Karachi, Peshawar, Islamabad and Karachi) of Pakistan

Appendix

See Table 7.

Table 7 The *source* model parameters for active crustal faults located in Pakistan and surrounding region (GEM 2019)

ID	Name	Fault type	Length (km)	Slip rate			Dip angle	Rake angle	M_{max}
				Min	Mean	Max			
1	Zhob fault	Reverse	335.41	1	2	3	65	85	7.9
2	Tirich mir fault	Sinistral-Reverse	189.41	0.3	1.6	3	80	60	7.5
3	Reshun fault	Reverse	111.45	0.15	0.6	1	45.5	85	7.6
4	Karak thrust	Reverse	68.76	1	1.5	2	46.5	85	7.3
5	Karak thrust	Reverse	43.77	1	1.5	2	62.5	85	7
6	Reshun fault	Sinistral-Reverse	135.29	0.15	0.6	1	67.5	37	7.4
7	Main karakoram thrust	Reverse	129.81	0.15	0.6	1	65	82	7.4
8	Main karakoram thrust	Reverse	105.28	0.15	0.6	1	65	82	7.4
9	Main karakoram thrust	Reverse	121.52	0.15	0.6	1	65	87	7.4
10	Main mantle thrust	Dextral-Reverse	109.80	0.15	0.6	1	70	120	7.3
11	Sindak fault	Dextral	245.25	1	1.2	1.5	85	180	7.6
12	Dargai fault	Reverse	105.28	0.15	0.6	1	55	85	7.5
13	West NEH fault iran	Dextral	204.50	1	1.2	1.5	85	180	7.6
14	Main mantle thrust	Reverse	51.64	0.15	0.6	1	65	85	7.1
15	Northern fault	Reverse	68.12	0.15	0.6	1	65	85	7.2
16	Raikot fault	Reverse	142.71	0.15	0.6	1	65	85	7.5
17	Balakot Bagh fault	Reverse	64.38	0.15	0.6	1	52.5	85	7.3
18	Main boundary thrust east	Reverse	279.79	1	1.5	2	65	85	7.8
19	Khair-I-Murat fault	Reverse	128.03	1	1.5	2	55	85	7.5
20	Khair-I-Murat fault	Reverse	143.64	1	1.5	2	65	85	7.5
21	Nowshera fault	Reverse	123.83	0.15	0.6	1	65	85	7.4
22	Punjal thrust	Reverse	227.01	1	1.5	2	65	85	7.7
23	Kalabagh fault	Dextral	41.97	1	1.5	2	65	177	6.9
24	Salt range thrust	Dextral-Reverse	63.64	1	1.5	2	67.5	120	7.1
25	Salt range thrust	Reverse	169.44	1	1.5	2	65	85	7.6
26	Karakuram fault	Normal	204.90	5.75	5	6.5	60	90	7.8
27	Salt range thrust	Reverse	158.90	1	1.5	2	65	85	7.6
28	Kurram thrust	Reverse	72.39	1	1.5	2	65	85	7.2
29	Main boundary thrust west	Reverse	104.61	1	1.5	2	65	85	7.4
30	Kingri fault	Sinistral-Reverse	111.01	1	2	3	70	30	7.3
31	Shingar fault	Reverse	86.59	1	2	3	65	85	7.3

Table 7 (continued)

ID	Name	Fault type	Length (km)	Slip rate			Dip angle	Rake angle	M_{max}
				Min	Mean	Max			
32	Murgha Kibzai fault	Reverse	124.22	1	2	3	65	85	7.4
33	Mekhtar fault	Reverse	202.56	1	2	3	65	85	7.7
34	Bar khan fault	Reverse	139.88	1	2	3	65	85	7.5
35	Pir koh fault	Reverse	236.83	1	2	3	65	85	7.7
36	Mach and johan fault	Reverse	96.68	1	2	3	65	85	7.4
37	Ghazaband fault	Sinistral	193.97	1	3	5	67.5	0	7.7
38	Ghazaband fault	Sinistral-Reverse	128.55	1	1.8	2.5	67.5	37	7.5
39	Gandava fault	Sinistral-Reverse	133.35	1	1.5	2	70	30	7.4
40	Ornach-Nal fault	Sinistral-Reverse	247.78	1	3	5	67.5	37	7.8
41	Nagar Parkar fault	Normal	540.70	0.15	1.6	3	65	272	8.1
42	Un-named fault	Normal	360.48	1	2	3	65	272	7.9
43	Ghazaband fault	Sinistral	285.16	1	3	5	67.5	0	7.9
44	Bazdar fault	Reverse	495.65	1	1.5	2	65	85	7.8
45	Chaman fault	Sinistral-Reverse	429.21	4	6	8	67.5	37	8
46	Dijabba fault	Reverse	107.44	1	1.5	2	65	85	7.4
47	Batal Thrust	Reverse	38.00	0.1	0.5	0.8	65	85	6.9
48	Panjal thrust	Reverse	54.43	0.15	0.6	1	65	85	7.1
49	Balakot shear zone	Sinistral-Reverse	21.09	0.1	0.6	1	67.5	37	6.6
50	Main mantle thrust	Reverse	107.32	0.15	0.5	0.8	65	85	7.4
51	Hoshab fault	Sinistral-Reverse	498.28	1	1.5	2	80	60	8
52	Gichk fault	Sinistral-Reverse	252.84	1	1.5	2	80	60	7.8
53	Panjgur fault	Sinistral-Reverse	253.56	1	1.5	2	80	60	7.7
54	Kirthar fault	Sinistral-Reverse	172.77	1	1.5	2	80	60	7.5
55	Zardak fault	Sinistral-Reverse	113.18	1	1.5	2	80	60	7.3
56	Nusratabad fault, Iran	Dextral	172.66	1	1.2	1.5	85	180	7.5
57	Panjgur fault	Reverse	234.66	1	1	1	65	90	7.7
58	Un-named fault	Reverse	206.82	1	1	1	52.5	90	7.8
59	Un-named fault	Dextral	132.82	1	1	1	80	180	7.4
60	Un-named fault	Dextral-Reverse	104.11	0.69	0.8	1	70	150	7.3
61	Un-named fault	Dextral-Reverse	105.74	1	1	1	70	150	7.3
62	Un-named fault	Reverse	212.26	1	1	1	45	90	7.9

Table 7 (continued)

ID	Name	Fault type	Length (km)	Slip rate			Dip angle	Rake angle	M_{max}
				Min	Mean	Max			
63	Un-named fault	Reverse	183.48	1	1	1	45	90	7.8
64	Un-named fault	Sinistral-Reverse	78.79	0.73	0.9	1	70	30	7.2
65	Un-named fault	Sinistral-Reverse	100.70	0.66	0.8	1	60	60	7.4
66	Un-named fault	Reverse	219.18	1	1	1	45	90	7.9
67	Un-named fault	Sinistral-Reverse	153.79	1	1	1	70	30	7.4
68	Mashkhel fault	Dextral-Reverse	348.89	1.5	1.9	2.21	70	150	7.8
69	Un-named fault	Reverse	180.82	1	1	1	45	90	7.8
70	Turbat fault	Reverse	358.20	1	1	1	45	90	8.1
71	Un-named fault	Reverse	173.92	1	1	1	45	90	7.8
72	Himalayan frontal thrust	Reverse	319.58	10	15	21	60	90	8
73	Main frontal thrust	Reverse	416.75	10	15	21	60	90	8.1
74	Karakuram fault	Dextral	403.04	1	6	11	60	90	8.2
75	Altyn tagh fault	Sinistral	692.52	4	7	10	60	90	8.4
76	Panjshir fault	Normal	419.44	2	3	4	60	275	8.1
77	Darvaz fault	Sinistral-Normal	407.11	2	3	4	70	315	8
78	Main karakuram thrust	Normal	239.04	1	1.5	2	80	275	7.7
79	Herat fault	Dextral	401.70	0.75	1.9	3	70	170	8.1
80	Herat fault	Reverse	50.26	0.2	1.1	2	70	70	7.1
81	Chaman fault	Sinistral-Normal	168.65	1	2.5	4	70	315	7.7
82	Chaman fault	Sinistral-Normal	211.27	1	3.4	5.8	70	315	7.8
83	Chaman fault	Sinistral-Normal	171.39	1	3.5	6	70	315	7.6
84	Chaman fault	Sinistral-Normal	142.32	1	2.2	3.5	70	315	7.6
85	Chaman fault	Sinistral-Normal	137.90	1	2.2	3.5	70	315	7.6
86	Chaman fault	Sinistral-Normal	92.85	1	3.5	6	70	315	7.4
87	Herat fault	Normal	98.92	0.2	1.1	2	70	272	7.4
88	Main karakoram thrust	Sinistral-Reverse	111.68	0.15	0.6	1	67.5	37	7.4
89	Main mantle thrust	Sinistral	45.09	0.15	0.6	1	70	0	6.9
90	Main mantle thrust	Reverse	34.95	0.15	0.6	1	65	85	6.9
91	Kashmir valey fault	Reverse	48.68	0.15	0.6	1	65	85	7.1
92	Jhelum fault	Reverse	50.49	0.15	0.6	1	55	104	7.1

Table 7 (continued)

ID	Name	Fault type	Length (km)	Slip rate			Dip angle	Rake angle	M_{max}
				Min	Mean	Max			
93	Balakot shear zone	Reverse	26.95	0.5	0.8	1	55	104	6.8
94	Panjal fault	Reverse	44.99	0.15	0.6	1	65	85	7
95	Riwat thrust	Reverse	80.79	0.15	0.6	1	65	85	7.3
96	Kurram thrust	Reverse	153.71	1	1.5	2	65	85	7.5
97	Nusratabad fault, Iran	Dextral	80.92	0.5	0.8	1	85	180	7.2
98	Zhob fault	Reverse	92.71	1	1.5	2	65	85	7.3
99	Nusratabad fault, Iran	Dextral	63.45	0.5	0.8	1	85	180	7.1
100	Un-named fault	Normal	202.26	1	2	3	65	272	7.6
101	Ziarat fault	Reverse	127.70	1	2	3	65	85	7.4
102	Shingar fault	Reverse	76.99	1	2	3	65	85	7.3
103	Bibi fault	Reverse	91.56	1	1.5	2	65	85	7.4
104	Un-named fault	Normal	323.91	1	1.5	2	65	272	7.8
105	Kachchh main-land fault	Normal	261.97	0.15	1.6	3	65	272	7.8
106	Hub fault	Reverse	324.27	1	2	3	65	85	7.9
107	East NEH fault Iran	Dextral	137.96	1	1.2	1.5	85	180	7.4
108	Gichk fault	Reverse	75.88	1	1.5	2	65	85	7.4
109	Reshun fault	Reverse	98.28	0.15	0.6	1	55	85	7.4
110	Reshun fault	Sinistral-Reverse	70.83	0.15	0.6	1	65	37	7.2

Acknowledgements The authors are very thankful to Prof. Dr. Pennung Warnitchai of Asian Institute of Technology (AIT, Thailand) for his invaluable guidance, training and suggestions. The study would not have been possible without his support.

References

Ahmad S, Hassan S, Mehnood K, Maqsood T (2018) Role of Chaman transform boundary fault in the deformation of Eastern Kharan Fore-Arc Basin. J Himal Earth Sci 51(1):75–98

Aitchison JC, Ali JR, Davis AM (2007) When and where did India and Asia collide? J Geophys Res Solid Earth. https://doi.org/10.1029/2006jb004706

Aki K (1965) Maximum likelihood estimate of b in the formula log N= a-bM and its confidence limits. . Bull Earthq Res Inst Tokyo Univ 43:237–239

Aki K (1988) Probabilistic seismic hazard analysis. National Academies, US

Akkar S, Çağnan Z (2010) A local ground-motion predictive model for Turkey, and its comparison with other regional and global ground-motion models. Bull Seismol Soc Am 100:2978–2995

Akkar S, Çağnan Z, Yenier E, Erdoğan Ö, Sandıkkaya MA, Gülkan P (2010) The recently compiled Turkish strong motion database: preliminary investigation for seismological parameters. J Seismol 14:457–479. https://doi.org/10.1007/s10950-009-9176-9

Akkar S, Sandıkkaya M, Bommer J (2014) Empirical ground-motion models for point-and extended-source crustal earthquake scenarios in Europe and the Middle East. Bull Earthq Eng 12:359–387

Aldama Bustos G (2009) An exploratory study of parameter sensitivity, representation of results and extensions of PSHA Emirates. Imperial College, London
Ali M (2011) Seismic hazard analysis of Pakistan. Pakistan Institute of Engineering and Applied Sciences, Nilore, Islamabad, Pakistan
Ambraseys N (2000) Reappraisal of north-Indian earthquakes at the turn of the 20th century. Curr Sci Bangalore 79:1237–1250
Ambraseys N, Bilham R (2014) The tectonic setting of Bamiyan and seismicity in and near Afghanistan for the past twelve centuries. In: Margottini Claudio (ed) After the destruction of Giant Buddha Statues in Bamiyan (Afghanistan) in 2001. Springer, Berlin, pp 101–152
Ambraseys N, Douglas J, Sarma S, Smit P (2005) Equations for the estimation of strong ground motions from shallow crustal earthquakes using data from Europe and the Middle East: horizontal peak ground acceleration and spectral acceleration. Bull Earthq Eng 3:1–53. https://doi.org/10.1007/s10518-005-0183-0
Ambraseys NN, Douglas J (2004) Magnitude calibration of north Indian earthquakes. Geophys J Int 159:165–206. https://doi.org/10.1111/j.1365-246x.2004.02323.x
Anderson JG (1979) Estimating the seismicity from geological structure for seismic-risk studies. Bull Seismol Soc Am 69:135–158. https://doi.org/10.1016/0148-9062(79)90309-7
Anderson JG, Luco JE (1983) Consequences of slip rate constraints on earthquake occurrence relations. Bull Seismol Soc Am 73:471–496
Arnaud NO, Brunel M, Cantagrel JM, Tapponnier P (1993) High cooling and denudation rates at Kongur Shan, Eastern Pamir (Xinjiang, China) revealed by 40Ar/39Ar alkali feldspar thermochronology. Tectonics 12:1335–1346. https://doi.org/10.1029/93tc00767
Atkinson GM, Boore DM (2003) Empirical ground-motion relations for subduction-zone earthquakes and their application to Cascadia and other regions. Bull Seismol Soc Am 93:1703–1729. https://doi.org/10.1785/0120020156
Atkinson GM, Boore DM (2006) Earthquake ground-motion prediction equations for eastern North America. Bull Seismol Soc Am 96:2181–2205
Atkinson GM, Boore DM (2011) Modifications to existing ground-motion prediction equations in light of new data. Bull Seismol Soc Am 101:1121–1135. https://doi.org/10.1785/0120100270
Bangash M (2011) Earthquake resistant buildings: dynamic analyses, numerical computations, codified methods, case studies and examples. Springer, Germany
Bannert D, Raza HA (1992) The segmentation of the indo-Pakistan plate. Pak J Hydrocarb Res 4:5–18
BCP (2007) Building code of Pakistan, seismic provision- 2007. Ministry of housing and works, Islamabad, Pakistan
Bommer JJ, Georgallides G, Tromans I (2001) Is there a near-field for small-to-moderate magnitude earthquakes? J Earthq Eng 5:395–423
Boore DM, Atkinson GM (2008) Ground-motion prediction equations for the average horizontal component of PGA, PGV, and 5%-damped PSA at spectral periods between 0.01 s and 10.0 s. Earthq Spectra 24:99–138. https://doi.org/10.1193/1.2830434
Boore DM, Joyner WB, Fumal TE (1997) Equations for estimating horizontal response spectra and peak acceleration from western North American earthquakes: a summary of recent work. Seismol Res Lett 68:128–153
Bozorgnia Y et al (2014) NGA-West2 research project. J Earthq Spectra 30:973–987
Byrne DE, Sykes LR, Davis DM (1992) Great thrust earthquakes and aseismic slip along the plate boundary of the Makran subduction zone. J Geophys Res Solid Earth 97:449–478. https://doi.org/10.1029/91jb02165
Campbell KW (2003) Prediction of strong ground motion using the hybrid empirical method and its use in the development of ground-motion (attenuation) relations in eastern North America. Bull Seismol Soc Am 93:1012–1033
Campbell KW, Bozorgnia Y (2008) NGA ground motion model for the geometric mean horizontal component of PGA, PGV, PGD and 5% damped linear elastic response spectra for periods ranging from 0.01 to 10 s. Earthq spectra 24:139–171. https://doi.org/10.1193/1.2857546
Campbell KW, Bozorgnia Y (2014) NGA-West2 ground motion model for the average horizontal components of PGA, PGV, and 5% damped linear acceleration response spectra. Earthq Spectra 30:1087–1115. https://doi.org/10.1193/062913eqs175m
Chen Z et al (2000) Global positioning system measurements from eastern Tibet and their implications for India/Eurasia intercontinental deformation. J Geophys Res Atmos 105:16215–16227. https://doi.org/10.1029/2000jb900092
Chiou B-J, Youngs RR (2008) An NGA model for the average horizontal component of peak ground motion and response spectra. Earthq Spectra 24:173–215. https://doi.org/10.1193/1.2894832

Chiou BS-J, Youngs RR (2014) Update of the Chiou and Youngs NGA model for the average horizontal component of peak ground motion and response spectra. Earthq Spectra 30:1117–1153. https://doi.org/10.1193/072813eqs219m
Cornell CA (1968) Engineering seismic risk analysis. Bull Seismol Soc Am 58:1583–1606
Danciu L et al (2018) The 2014 earthquake model of the middle east: seismogenic sources. Bull Earthq Eng 16:3465–3496. https://doi.org/10.1007/s10518-017-0096-8
DeMets C, Gordon RG, Argus D, Stein S (1990) Current plate motions. Geophys J Int 101:425–478. https://doi.org/10.1111/j.1365-246x.1990.tb06579.x
Durrani AJ, Elnashai AS, Hashash YMA, Kim SJ, Masud A (2005) The Kashmir earthquake of october 08, 2005. Mid-America Earthquake Center, United States
Frankel A (1995) Mapping seismic hazard in the central and eastern United States. Seismol Res Lett 66:8–21. https://doi.org/10.1785/gssrl.66.4.8
Gardner J, Knopoff L (1974) Is the sequence of earthquakes in Southern California, with aftershocks removed, Poissonian? Bull Seismol Soc Am 64:1363–1367
GEM (2019) GEM Global active faults. https://blogs.openquake.org/hazard/global-active-fault-viewer/. Accessed 15th July 2019
Giardini D (1999) The global seismic hazard assessment program (GSHAP)-1992/1999. Ann Geophys. https://doi.org/10.4401/ag-3780
Giardini D, Basham P (1993) Technical guidelines for global seismic hazard assessment. Ann Geophys. https://doi.org/10.4401/ag-4257
Giardini D, Grünthal G, Shedlock KM, Zhang P (1999) The GSHAP global seismic hazard map. Ann Geophys. https://doi.org/10.4401/ag-3784
Gutenberg B, Richter CF (1944) Frequency of earthquakes in California. Bull Seismol Soc Am 34:185–188
Gutenberg B, Richter CF (1956) Earthquake magnitude, intensity, energy, and acceleration: (Second paper). Bull Seismol Soc Am 46:105–145
Hanks TC, Kanamori H (1979) A moment magnitude scale. J Geophy Res Solid Earth 84:2348–2350. https://doi.org/10.1029/jb084ib05p02348
Heaton TH, Tajima F, Mori AW (1986) Estimating ground motions using recorded accelerograms. Surv Geophys 8:25–83. https://doi.org/10.1007/bf01904051
Huo J, Hu Y (1992) Study on attenuation laws of ground motion parameters. Earthq Eng Eng Vib 12:1–11
ISC (2019) http://www.isc.ac.uk/iscbulletin/search/catalogue/. Accessed 15th April 2019
Kazmi AH, Jan MQ (1997) Geology and tectonics of Pakistan. Graphic publishers, Karachi
Khan MA et al (2008) Preliminary geodetic constraints on plate boundary deformation on the western edge of the Indian plate from TriGGnet (Tri-University GPS Geodesy Network). J Himal Earth Sci 41:71–87
Khan S, Waseem M, Khan MA, Ahmed W (2018) Updated earthquake catalogue for seismic hazard analysis in Pakistan. J Seismol 22:841–861. https://doi.org/10.1007/s10950-018-9736-y
Kulkarni R, Youngs R, Coppersmith K (1984) Assessment of confidence intervals for results of seismic hazard analysis. In 8th world conference on earthquake engineering
Lapajne J, Motnikar BS, Zupancic P (2003) Probabilistic seismic hazard assessment methodology for distributed seismicity. Bull Seismol Soc Am 93:2502–2515
Lapajne JK, Motnikar BS, Zabukovec B, Zupancic P (1997) Spatially smoothed seismicity modeling of seismic hazard in Slovenia. J Seismol 1:73–85
Lin P-S, Lee C-T (2008) Ground-motion attenuation relationships for subduction-zone earthquakes in northeastern Taiwan. Bull Seismol Soc Am 98:220–240
Magsi HZ (2014) Relation of seismicity with surface faults in Pakistan: an overview. NCGT J 2:42–55
McClusky S, Reilinger R, Mahmoud S, Ben Sari D, Tealeb A (2003) GPS constraints on Africa (Nubia) and Arabia plate motions. Geophys J Int 155:126–138. https://doi.org/10.1046/j.1365-246x.2003.02023.x
McGuire RK (1976) FORTRAN computer program for seismic risk analysis. US Geol Surv. https://doi.org/10.3133/ofr7667
McGuire RK (1978) FRISK: computer program for seismic risk analysis using faults as earthquake sources. Open-File Report US Geological Survey
Musson R (2009) Subduction in the Western Makran: the historian's contribution. J Geol Soc 166:387–391. https://doi.org/10.1144/0016-76492008-119
Negredo AM, Replumaz A, Villaseñor A, Guillot S (2007) Modeling the evolution of continental subduction processes in the Pamir-Hindu Kush region. Earth Planet Sci Lett 259:212–225. https://doi.org/10.1016/j.epsl.2007.04.043

Ornthammarath T, Warnitchai P, Worakanchana K, Zaman S, Sigbjörnsson R, Lai CG (2011) Probabilistic seismic hazard assessment for Thailand. Bull Earthq Eng 9:367–394. https://doi.org/10.1007/s10518-010-9197-3

Pagani M et al (2014) OpenQuake engine: an open hazard (and risk) software for the global earthquake model. Seismol Res Lett 85:692–702. https://doi.org/10.1785/0220130087

PBC (1986) Building code of Pakistan. Ministry of housing and works, Government of Pakistan, Pakistan

Petersen MD et al (2008) Documentation for the 2008 update of the United States national seismic hazard maps. Geol Surv US. https://doi.org/10.3133/ofr20081128

Petersen MD et al (2015) The 2014 United States national seismic hazard model. Earthq Spectra 31:S1–S30

PMD, NORSAR (2007) Seismic hazard analysis and zonation of Pakistan, Azad Jammu and Kashmir. Pakistan Meteorological Department

Quittmeyer R, Jacob K (1979) Historical and modern seismicity of Pakistan, Afghanistan, northwestern India, and southeastern Iran. Bull Seismol Soc Am 69:773–823

Rafi Z, Lindholm C, Bungum H, Laghari A, Ahmed N (2012) Probabilistic seismic hazard of Pakistan, Azad-Jammu and Kashmir. Nat Hazards 61:1317–1354. https://doi.org/10.1007/s11069-011-9984-4

Regard V et al (2010) The transition between Makran subduction and the Zagros collision: recent advances in its structure and active deformation. Geol Soc Lond Spec Publ 330:43–64. https://doi.org/10.1144/sp330.4

Rossetto T, Peiris N (2009) Observations of damage due to the Kashmir earthquake of October 8, 2005 and study of current seismic provisions for buildings in Pakistan. Bull Earthq Eng 7:681–699

Rydelek PA, Sacks IS (1989) Testing the completeness of earthquake catalogues and the hypothesis of self-similarity. Nature 337:251

Sawires R, Santoyo MA, Peláez JA, Corona Fernández RD (2019) An updated and unified earthquake catalog from 1787 to 2018 for seismic hazard assessment studies in Mexico. Sci Data 6:241. https://doi.org/10.1038/s41597-019-0234-z

Searle M (2013) Colliding continents: a geological exploration of the Himalaya, Karakoram, and Tibet. Oxford University Press, UK

Şeşetyan K et al (2018) The 2014 seismic hazard model of the Middle East: overview and results. Bull Earthq Eng 16:3535–3566. https://doi.org/10.1007/s10518-018-0346-4

Shabbir MJ, Ilyas M (2007) Development and adoption of building code of Pakistan. In: Proceedings of CBM-CI International Workshop, Karachi, Pakistan. pp 535–549

Shi Y, Bolt BA (1982) The standard error of the magnitude-frequency b value. Bull Seismol Soc Am 72:1677–1687

Stepp J (1973) Analysis of completeness of the earthquake sample in the Puget Sound area. NOAA Tech. Report ERL 267-ESL30, Boulder, Colorado

Stirling MW, Wesnousky SG, Shimazaki K (1996) Fault trace complexity, cumulative slip, and the shape of the magnitude-frequency distribution for strike-slip faults: a global survey. Geophys J Int 124:833–868. https://doi.org/10.1111/j.1365-246X.1996.tb05641.x

Stoneley R (1974) Evolution of the continental margins bounding a former southern Tethys. In: Burk Creighton A, Drake Charles L (eds) The geology of continental margins. Springer, Berlin, pp 889–903

Tinti S, Mulargia F (1985) Completeness analysis of a seismic catalog. Ann Geophys 3:407–414

Toro GR (2002) Modification of the Toro et al. (1997) attenuation equations for large magnitudes and short distances. Risk Engineering Technical Report

UBC (1997) Uniform building code international conference of building officials. Whittier, California

USGS (2019) https://earthquake.usgs.gov/earthquakes/search/. Accessed 10 April 2019

Utsu T (2002) A list of deadly earthquakes in the world: 1500–2000. In: Lee WHK, Kanamori H, Jennings PC, Kisslinger C (eds) International geophysics. Elsevier, Amsterdam, pp 691–691

Wells DL, Coppersmith KJ (1994) New empirical relationships among magnitude, rupture length, rupture width, rupture area, and surface displacement. Bull Seismol Soc Am 84:974–1002

Wiemer S (2001) A software package to analyze seismicity: ZMAP. Seismol Res Lett 72:373–382. https://doi.org/10.1785/gssrl.72.3.373

Youngs R, Chiou S-J, Silva W, Humphrey J (1997) Strong ground motion attenuation relationships for subduction zone earthquakes. Seismol Res Lett 68:58–73

Youngs RR, Coppersmith KJ (1985) Implications of fault slip rates and earthquake recurrence models to probabilistic seismic hazard estimates. Bull Seismol Soc Am 75:939–964

Zaman S, Ornthammarath T, Warnitchai P (2012) Probabilistic seismic hazard maps for Pakistan. In: Proceeding of the 15th World Conference in Earthquake Engineering-WCEE. pp 1–10

Zare M et al (2014) Recent developments of the Middle East catalog. J Seismolog 18:749–772. https://doi.org/10.1007/s10950-014-9444-1

Zhang P, Yang Z, Gupta HK, Bhatia SC, Shedlock KM (1999) Global seismic hazard assessment program (GSHAP) in continental Asia. Ann Geophys 42(6):1167–1190

Zhao JX et al (2006) Attenuation relations of strong ground motion in Japan using site classification based on predominant period. Bull Seismol Soc Am 96:898–913